Evolution of the long-term and estuary-scale phytoplankton patterns in the Scheldt estuary: the disappearance of net growth in the brackish region

Dante M. L. Horemans[1], Yoeri M. Dijkstra[2], Michèle Tackx[3], Patrick Meire[1], and Tom J. S. Cox[1,4]

[1]Ecosystem Management Research Group, University of Antwerp, Wilrijk, Belgium
[2]Delft Institute of Applied Mathematics, Delft University of Technology, Delft, Netherlands
[3]Laboratoire Ecologie Fonctionnelle et Environnement, Université de Toulouse, CNRS, Toulouse INP, Université Toulouse 3 - Paul Sabatier (UPS), Toulouse, France
[4]NIOZ Royal Netherlands Institute for Sea Research, Yerseke, Netherlands

Correspondence: Dante M. L. Horemans (dante.horemans@uantwerpen.be)

Abstract. Estuaries often show regions in which Chlorophyll-a (Chl-a) accumulates. The location and magnitude corresponding to such accumulation result from a complex interplay between processes such as river flushing, salinity, nutrients, phytoplankton grazing, and the light climate in the water column. Of particular interest is the long-term evolution of the estuary-scale Chl-a distribution in the Scheldt estuary (Belgium/Netherlands) in spring. From 2004-2007, we observed a limited spring-bloom in the brackish region. This bloom intensified in 2008-2014 and disappeared after 2015. This long-term evolution in Chl-a has been linked to simultaneous long-term trends in the suspended particulate matter (SPM) distribution and the improvement of the water quality, which affects grazing of Chl-a by zooplankton. However, this hypothesis has not been systematically investigated. In this paper, we apply two approaches to test this hypothesis. In the first approach, we analyze long-term in situ observations covering the full estuary. These observations include the SPM concentration, zooplankton abundance, and other variables affecting the Chl-a concentration, and show a long-term estuary-scale evolution in not only the SPM distribution but also in zooplankton abundance, freshwater discharge, and maximum photosynthetic rate. In the second approach, we apply a model approach supported by these observations to determine which of the changed conditions may explain the observed change in Chl-a. Our results suggest that a change in SPM alone cannot explain the Chl-a observations. Instead, mortality rate and grazing by zooplankton mainly explains the long-term estuary-scale evolution of Chl-a in spring. Our results highlight that insight into the zooplankton dynamics is essential to understand the phytoplankton (cf. Chl-a) dynamics in the Scheldt estuary.

1 Introduction

The Chlorophyll-a (Chl-a) concentrations in estuaries often show regions where Chl-a accumulates, resulting in zones with locally elevated Chl-a concentrations. Such accumulation results from a complex interplay between physical, transport-related processes and chemical-biotic processes that determine net local phytoplankton growth. Such processes include water temperature (Eppley, 1972), river flushing (Filardo and Dunstan, 1985; Liu and de Swart, 2015), salinity (Lucas et al., 1998),

phytoplankton grazing (Alpine and Cloern, 1992; Lionard et al., 2005a), nutrients (Tilman et al., 1982; Cira et al., 2016), and the light climate in the water column (Sverdrup, 1953; Desmit et al., 2005).

In turbid estuaries, the light climate in the water column is often the limiting factor of phytoplankton growth. Consequently, the dynamics of suspended particulate matter (SPM) that determine the light climate are crucial to understanding the phyto-
plankton dynamics. Examples of such light-limited systems are the Gironde estuary (Irigoien and Castel, 1997), Seine estuary (Garnier et al., 2001), Ems estuary (Liu et al., 2018), and Scheldt estuary (Desmit et al., 2005).

In view of the interplay between phytoplankton, SPM, and other factors, the Scheldt estuary is particularly interesting. Cox et al. (2019) reported a long-term estuary-scale change in SPM dynamics in the Scheldt estuary. From 2009 onwards, a change in the estuarine turbidity maximum dynamics and an overall increase in SPM concentration was observed. Simultaneously,
the water quality in the Scheldt estuary improved drastically mainly because of a significant increase in wastewater treatment capacity in Brussels around 2006 (Brion et al., 2015). This resulted in increasing oxygen concentrations and changes in the zooplankton community and abundance. More specifically, calanoid copepods, in casu *Eurytemora affinis*, which dominated in the downstream brackish region, but were quasi absent in the freshwater region at the beginning of the observations in 1996, gradually developed more upstream, to also become dominant there from 2009 (Appeltans, 2003; Mialet et al., 2010, 2011;
Chambord et al., 2016). This could affect the phytoplankton abundance through grazing.

These changes in the SPM dynamics and zooplankton abundance coincide with long-term changes in phytoplankton dynamics. Of particular interest is the appearance and disappearance of a phytoplankton spring bloom in the brackish region. From 2004 until 2007, we observed almost no spring-bloom in the brackish region. Such a spring bloom was consistently observed between 2008-2014 but disappeared after 2015. The reported changes in SPM and zooplankton dynamics have been hypoth-
esized to link to the long-term disappearance of phytoplankton blooms (Maris and Meire, 2017). However, this has not been systematically investigated, which is necessary given the complex interplay between factors affecting phytoplankton growth.

Therefore, to test this hypothesis and determine, besides the evolution in SPM concentration and zooplankton abundance, other potential causes that may explain the long-term disappearance of phytoplankton accumulation in the brackish zone of the Scheldt estuary, we apply two approaches. In the first approach, we analyze the long-term trends in observed SPM
concentrations and other variables that impact phytoplankton growth and may explain the long-term evolution of phytoplankton abundance in the Scheldt estuary. In the second approach, we apply an extensive model sensitivity analysis, supported by the long-term observations to disentangle the complex interplay of various factors affecting phytoplankton growth and quantify the impact of variability in these factors on phytoplankton abundance. The model approach also allows us to estimate parameters that are difficult to measure, such as the phytoplankton mortality rate. Here, we aim to determine the processes and complexity
that are essential to capture the observed phytoplankton abundance on the estuary-scale. To do so, we first assume a system-constant mortality rate to model the phytoplankton abundance. Next, we add more complexity to the model by making the mortality rate dependent on the abundance of zooplankton and grazing.

Biogeosciences
Discussions

2 Material and methods

In this section, we first introduce the Scheldt estuary. Next, the methodology to obtain the observations is discussed and the
55 model approach is presented.

2.1 Study area

The Scheldt estuary is a funnel-shaped estuary which flows through Belgium into the North Sea near Vlissingen (Netherlands)
over a distance of approximately 160 km (see Fig. 1). Given its relatively small freshwater discharge, the Scheldt estuary
is tide-dominated (Meire et al., 2005). The total time-averaged freshwater discharge Q in spring (Apr.-May) equals 85, 81,
60 and 72 m^3 s^{-1} in 2004-2007, 2008-2014, and 2015-2018, respectively (Waterinfo.be, cited 2019). The main tributaries of the
Scheldt estuary are the Rupel and the Dender. They are responsible for 64.2, 59.3, 63.3 % and 9.4, 9.2, 9.6 % of the total
river discharge in 2004-2007, 2008-2014, and 2015-2018, respectively (Waterinfo.be, cited 2019). The Scheldt estuary is a
nutrient-rich estuary (Maris and Meire, 2017). The dissolved nitrogen concentrations in spring range from 0.1 mmol L^{-1} at
the seaside boundary to 0.4 mmol L^{-1} at the upstream boundary. The dissolved phosphorous concentrations range from 0.001
65 mmol L^{-1} at the seaside boundary to 0.007 mmol L^{-1} at the upstream boundary. These concentrations are at least one order
of magnitude larger than the threshold values at which we expect nutrient depletion (Soetaert et al., 1994; Arndt et al., 2011;
Dijkstra et al., 2019a).

2.2 In situ observations

Both the Belgian and Dutch part of the Scheldt estuary have been monitored intensively over the last two decades. In the
70 Belgian region, various variables, including Chl-a, SPM, salinity, and phytoplankton characteristics, such as the maximum
phytoplankton production rate μ_{max} and growth efficiency α, have been measured within the long-term OMES (Dutch: "On-
derzoek Milieu Effecten Sigmaplan") monitoring campaign (Maris and Meire, 2017), independently of the tidal phase and
spring-neap tide bi-weekly or monthly at 16 fixed stations (see Fig. 1). In the Dutch region, we only use observations of Chl-
a and SPM by Rijkswaterstaat at three stations in the main channel (see Fig. 1). In the following, we briefly introduce the
75 methodology used to obtain the observations presented in this study. For a detailed methodological description, we refer the
reader to the OMES reports (Maris and Meire, 2017) and the official website of Rijkswaterstaat (Rijkswaterstaat, 2020).

2.2.1 Chl-a and zooplankton abundance

Within the OMES monitoring program, sub-surface bucket samples were taken to estimate the Chl-a concentration and the
mesozooplankton abundance between 2004-2018. The Chl-a concentration was estimated following the spectrophotometric
80 method described in Rice et al. (2017) that corrects for turbidity, chlorophyll b, chlorophyll c, and pheophytin pigments, using
50 ml water samples, a 1-cm pathway cuvette, and a Shimadzu UV-1700 spectrophotometer. The observations conducted
by Rijkswaterstaat in the Dutch part of the Scheldt estuary were estimated using High-performance liquid chromatography
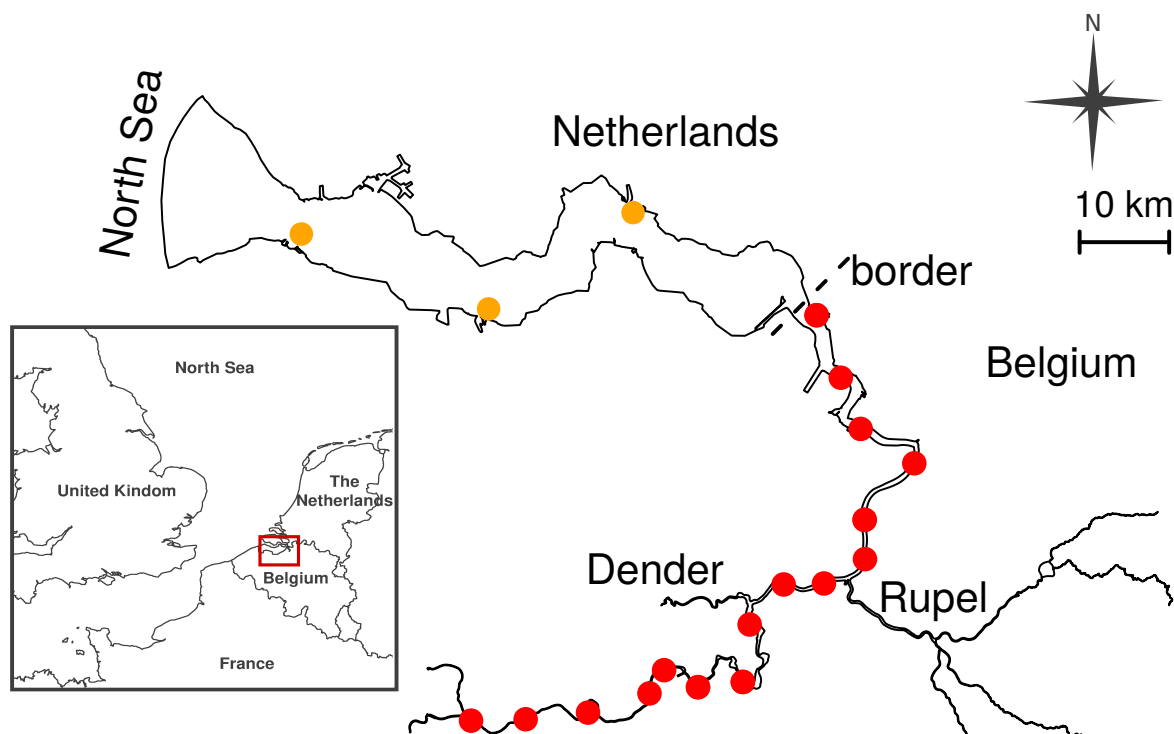(HPLC) after filtration and extraction.

Figure 1. The Scheldt estuary and its two main tributaries (Rupel and Dender). The red dots represent the locations where monthly and bi-weekly turbidity and floc size profiles were measured in the frame of the OMES environmental monitoring program. The orange dots depict the location of the observations conducted by Rijkswaterstaat.

To estimate the mesozooplankton abundance, 50-250 L sub-surface water samples were collected and filtered over a 50 μm
85 mesh. Next, the mesozooplankton was fixed using formaldehyde and stained with erythrosine in the laboratory. Finally, the organisms were counted in a counting wheel under a binocular microscope using a subsample. A minimum of 500 individuals per subsample was counted (Le Coz et al., 2017). Because in the brackish region in spring, which is the main focus of this paper, the mesozooplankton community dominantly consists of calanoids (Appeltans, 2003; Mialet et al., 2011), we divide the community in two groups: adult calanoids and non-calanoids (i.e., cladocerans, harpacticoids, and cyclopoids).

90 **2.2.2 Turbidity and SPM concentration**

Within the OMES campaign, turbidity depth-profiles were measured in 2015-2018 using an Optical Backscatter point Sensor (OBS) of RBR type XR420 CTD+ at the 16 OMES station. Simultaneously, two SPM samples were collected at approximately the water surface and half the water depth. These SPM samples were used to translate turbidity to SPM concentration (Horemans et al., 2020a). The number of campaigns in spring between 2015-2018 equals 16.

95   To determine the SPM concentration, 1 L water samples were collected and filtered in the laboratory. To remove salinity, the filters were rinsed with 3×50 ml demineralized water before gravimetrically determining the SPM concentrations (norm NBN-EN872). Also within the monitoring program of Rijkswaterstaat, SPM concentrations were gravimetrically determined after filtration on a glass microfiber filter.

2.2.3   Light extinction coefficients, temperature and salinity

100 The light climate was measured by estimating the light extinction coefficient k_d. Two light sensors (LiCOR) measured the light intensity near the water surface E_1 and the light-intensity E_2 at a fixed distance $\Delta z = 40$ cm from the sub-surface sensor. Next, the light extinction coefficient was estimated as $k_d = \log(E_1/E_2)/\Delta z$, assuming exponential decrease of light as a function of depth. To correct for small-scale temporal variability (cf. seconds) in the light climate, the time-averaged value of k_d was estimated over a time interval of 3-5 minutes, using a sampling frequency of 1 s^{-1} (Maris and Meire, 2017).

105   Temperature and specific conductivity were determined in situ using a WTW LF 318 instrument, directly after taking the bucket samples. Specific conductivity was transformed to salinity using the Practical Salinity Scale 1978 (Perkin and Lewis, 1980).

2.2.4   Photosyntetic parameters

To estimate the photosynthetic parameters $\mu_{\max}$ and α, the incubation method described in Kromkamp and Peene (1995) was
110 applied using the incubator presented in Vegter and De Visscher (1984) and assuming a photosynthesis-irradiance (P-I) curve introduced in Eilers and Peeters (1988). Briefly, water samples were placed at fixed distances from a constant light source. Each distance thus corresponds to a given solar irradiance I. Next, the water samples were incubated for approximately 2 hours, while gently being rotated to avoid settling. The productivity P was determined using a C-14 isotope method, after which a P-I curve was constructed to estimate $\mu_{\max}$ and α.

115 ## 2.3   Model experiments

2.3.1   iFlow model

The model we use is the process-based, width-averaged, idealized model called iFlow (Dijkstra et al., 2017). The model solves for water motion and cohesive SPM trapping in tide-dominated estuaries by resolving the width-averaged shallow water and SPM mass balance equations in equilibrium condition. The flocculation dynamics of cohesive SPM are resolved using a single-
120 class dynamic flocculation model (Winterwerp, 2002; Horemans et al., 2020a). The model focuses on the estuary-scale hydro- and SPM dynamics only by approximating the estuary's bathymetry and width by smooth profiles. The model resolves the tidal and subtidal water motion and cohesive SPM concentration and provides approximate solutions of the complex and non-linear set of equations for hydro- and SPM dynamics using a scaling and perturbation approach.

    The hydrodynamics are forced at the upstream boundary and two main tributaries by a fixed water inflow and at the mouth by
125 a tidal signal. Following Warner et al. (2005), the longitudinal salinity profile is implemented as a tide- and depth-independent

profile (see Appendix A). This assumption is consistent with the Scheldt estuary being a well-mixed estuary. The SPM dynamics are forced by a constant inflow of SPM that equals the product of the water discharge and subtidal SPM concentration at the upstream boundary, and by a fixed SPM concentration at the mouth. We assume that erosion of sediment scales to the magnitude of the bed shear stress. For details on the performance of this model for the Scheldt estuary, we refer to Horemans et al.

130 (2020a). For this study, it suffices to mention that the M2 tidal and subtidal surface elevation correspond well to observations and that the magnitude of the SPM concentration and ETM location are reproduced.

The iFlow model has recently been extended by a phytoplankton model (Dijkstra et al., 2019a). The phytoplankton model is a dynamic model that describes the spatial and tidal evolution of phytoplankton concentration and the nutrients nitrogen and phosphorous. We do not focus on the equation for the nutrient dynamics because the Scheldt estuary can be considered

135 a nutrient-rich system, as mentioned above. However, we solve the nutrient dynamics in the model as done by Dijkstra et al. (2019a) to guarantee that we do not falsely neglect nutrient depletion in the extreme limits in our sensitivity analysis. The model consists of a single-phytoplankton class and thus does not differentiate between diatoms and non-diatoms. Consequently, Si-dynamics and salinity stress are not included and phytoplankton characteristics are assumed to be constant in the system. For completeness, we repeat the width-averaged differential equation for the phytoplankton dynamics P and corresponding

140 boundary conditions (Dijkstra et al., 2019a):

$$\underbrace{\partial_t P + u\partial_x P + (w - w_P)\partial_z P - \frac{1}{B}\partial_x(BK_h\partial_x P) - \partial_z(K_\nu\partial_z P)}_{\text{advection-diffusion}} = \underbrace{(\mu - m)P}_{\text{balance between local growth and mortality}}, \tag{1}$$

$$\begin{cases} w_P P + K_\nu\partial_z P = 0, & \text{at the bed and water surface (no flux),} \\ \left\langle \frac{1}{H}\int_{-H}^{\zeta} Pdz \right\rangle = P_{\text{sea}}, & \text{at the seaside boundary (constant concentration),} \\ B\left\langle \int_{-H}^{\zeta}(uP - K_h\partial_x P)dz \right\rangle = QP, & \text{at the upstream boundary (constant influx),} \end{cases} \tag{2}$$

in which t represents time, x and z are the coordinates in longitudinal and vertical direction, u and w are the water velocities in longitudinal and vertical direction, w_P is the constant settling velocity of phytoplankton cells, B is the width of the

145 Scheldt estuary, K_h and K_ν are the horizontal and vertical eddy diffusivities, $\langle\cdot\rangle$ denotes averaging over a long timescale (i.e., larger than a tide or day), $-H$ and ζ are the z-coordinates of the bed and water surface, P_{sea} is the constant phytoplankton concentration at the seaside boundary, QP is the constant influx of phytoplankton at the upstream boundary, and μ and m are the growth and mortality rate of phytoplankton. To determine the processes and complexity that are essential to capture the observed phytoplankton abundance, different choices for the mortality rate can be made. The simplest choice is to apply an

150 estuary-constant mortality rate m_0. However, in the literature, multiple extensions of the mortality rate have been studied. As a start, we consider the following simple longitudinal variation in m due to zooplankton abundance:

$$m = \begin{cases} m_0, & \text{default case,} \\ g_1 \cdot Z^{\text{calanoids}}(x) + g_2 \cdot Z^{\text{non-calanoids}}(x), & \text{extension (Section 3.2.4),} \end{cases} \tag{3}$$

in which $Z^{\text{calanoids}}$ and $Z^{\text{non-calanoids}}$ are the calanoids and non-calanoids zooplankton abundances, respectively, and m_0, g_1, and

g_2 are coefficients that follow from calibration. The magnitude of these scaling factors g_1 and g_2 reflect the grazing efficiency of

155 phytoplankton by zooplankton. For the implementation of the (time-averaged) growth rate μ, we follow Dijkstra et al. (2019a)

but use the Plat light limitation function (Platt et al., 1980). The reason is that, to further decrease the computational cost and

also include the impact of temporal variability in water depth on phytoplankton productivity, we use the approximated Platt

light-limitation function presented in Horemans et al. (2020b). Without nutrient limitation, μ then reads

$$\mu = \mu_{\text{max}}(T) \left\langle \underbrace{\left[1 - \exp\left(\frac{\alpha}{\mu_{\text{max}}} E \right) \right]}_{\text{Platt light limitation}} \right\rangle, \tag{4}$$

160 in which T is the water temperature and E is the photosynthetic active radiation (PAR):

$$E(z,t;P,c) = E_{00}(t) \underbrace{\exp\left(k_{\text{bg}}z - k_c \int_z^0 c(z,t)dz - k_P \int_z^0 P(z,t)dz \right)}_{\text{Lambert-Beer light extinction}} \times \underbrace{\begin{cases} \sin\left(\omega_E t \right) & \text{if } 0 < t < \pi/\omega_E \\ 0 & \text{elsewhere} \end{cases}}_{\text{truncated sinusoid representing the day/night cycle}}, \tag{5}$$

in which E_{00} represents the maximum PAR during mid-day (which varies on a seasonal time-scale), k_{bg}, k_c, and k_P are

the background, sediment-induced, and phytoplankton-induced exponential light extinction coefficients, respectively, c is the

SPM concentration, and ω_E is the angular frequency for day length. Following Eppley (1972), we postulate the following

165 temperature dependence of the maximum growth rate $\mu_{\text{max}}(T)$:

$$\mu_{\text{max}}(T) = \mu_{00} \cdot \mu_{01}^T, \tag{6}$$

in which μ_{00} and μ_{01} are calibration parameters.

As with the hydro- and SPM dynamics, the model solves the approximated phytoplankton dynamics in equilibrium conditions using a scaling and perturbation method (Dijkstra et al., 2019a). This method, in combination with the approximated Platt

170 light-limitation function, drastically decreases computation time, allowing for an extensive sensitivity analysis.

2.3.2 Sensitivity analysis

To determine potential environmental changes that may have caused the disappearance of phytoplankton accumulation in the

brackish region, we apply an extensive sensitivity study which is supported by observations. To this end, we first determine a

reference case that represents spring conditions in 2004-2007, 2008-2014, and 2015-2018. Here, most model parameter values

175 directly follow from observations. Using the μ_{max} and temperature observations, we derive the calibration parameters μ_{00} and

μ_{01} which contain the temperature dependence of μ_{max} [Eq. (6), see Appendix B for a calibration]. Following Horemans et al.

(2020a), to correct for the large temporal variability in discharges (Waterinfo.be, cited 2019) and correctly resolve the sediment

dynamics in spring, we calibrate the freshwater discharge and we determine the erosion and flocculation characteristics by

calibrating the modeled residual SPM distribution to the in situ turbidity observations using a cost function which is based

180 on a two-tailed t-test. This calibration results in a representative modeled SPM distribution in 2004-2007, 2008-2014, and 2015-2018. We refer the reader to Appendix C for the technical details. To ensure that we correctly model light extinction, we use these modeled SPM distributions in combination with the observations of the light extinction coefficient k_d to estimate the sediment-induced light extinction coefficient k_c (see Appendix D for the technical details). The influx of phytoplankton at the upstream boundary QP, system-constant mortality rate m_0, and grazing efficiencies g_1 and g_2 corresponding to the calanoids

185 and non-calanoids, respectively, are estimated by calibrating modeled Chl-a concentrations to the Chl-a observations. Here, we again use the calibration method described in Horemans et al. (2020a) in which the phytoplankton model results and observations (cf. Chl-a) are quantitatively compared. The model parameters that are the focus of this paper are summarized in Table 1. The full parameter list is listed in the Supporting Information attached to this paper. The reported values follow from observations, calibration, Dijkstra et al. (2019a), and Horemans et al. (2020a).

Table 1. Parameter values used in our model experiments based on observations (source), model calibration (calibrated), and the literature. If only one parameter value is presented, we used this value for all three periods.

variable	definition	value			unit
		2004-2007	2008-2014	2015-2018	
μ_{00}	calibration parameter in postulated temperature dependence for $\mu_{\max}$ (source)	1.12×10^{-5}	1.21×10^{-5}	1.00×10^{-5}	s^{-1}
μ_{01}	calibration parameter in postulated temperature dependence for $\mu_{\max}$ (source)	1.10	1.07	1.05	/
$\mu_{\max} : \alpha$	ratio between maximum photosynthetic rate and growth efficiency (source)	393	381	230	μmol photons m^{-2} s^{-1}
m_0	phytoplankton mortality rate (calibrated)	0.83×10^{-6}	1.19×10^{-6}	2.64×10^{-6}	s^{-1}
g_1	calanoids grazing efficiency (calibrated)	1.6×10^{-7}	0.24×10^{-7}	1.6×10^{-7}	s^{-1} L
g_2	non-calanoids grazing efficiency (calibrated)	0.93×10^{-7}	0.63×10^{-7}	0.93×10^{-7}	s^{-1} L
E_{00}	maximum PAR (source)		1007		μmol photons m^{-2} s^{-1}
ω_E	angular frequency for day length (source)		0.215		d^{-1}
T	water temperature (source)	14.3	14.7	14.7	$^\circ$ C
P_{sea}	phytoplankton boundary concentration at the mouth (source)	15.9	17.1	15.8	μg L^{-1}
QP	influx of phytoplankton at the upstream boundary (calibrated)	1.5	1.8	2.5	g s^{-1}
w_P	settling velocity of phytoplankton cells (Dijkstra et al., 2019a)		1.15×10^{-5}		m s^{-1}
k_{bg}	background exponential light extinction coefficient (Dijkstra et al., 2019a)		0.095		m^{-1}
k_P	phytoplankton-induced exponential light extinction coefficient (Dijkstra et al., 2019a)		18		m^2 (mol N)$^{-1}$
k_c	sediment-induced exponential light extinction coefficient (source)	81.4	77.9	72.0	m^2 kg^{-1}

190 **3 Results**

In this section, we first show the long-term observations of Chl-a and factors impacting phytoplankton growth in the Scheldt estuary in spring. Next, we present the results of our model experiments: we calibrate the model and apply an extensive sensitivity analysis of factors that may explain the disappearance of phytoplankton accumulation in the brackish region.

3.1 Evolution of Chl-a and corresponding environmental conditions of the in situ observations

195 ### 3.1.1 Evolution in Chl-a and zooplankton

Figure 2 shows the evolution of the Chl-a concentration in 2004-2018, indicating a clear seasonality with corresponding phytoplankton blooms; at the upstream boundary, the Chl-a concentration can reach values above 400 μg L^{-1} in summer and, although local maxima are observed, decays in the downstream direction. We divide the time series in three distinct periods. In 2004-2007, we find Chl-a concentrations above 50 μg L^{-1} in the upstream region, > km 80. In 2008-2014 and 2015-2018,

200 this region is limited to > 100 km and > 110 km, respectively. In 2008-2014, we also observe concentrations > 50 μg L^{-1} more downstream between km 40-80 in spring (Apr.-May).

Figure 3 shows the time-averaged Chl-a concentration and the calanoids and non-calanoids abundance in spring for the three distinct periods considered. The error bars and shaded area depict the standard error of the Chl-a observations and zooplankton abundance, respectively. The calanoids abundance (see Fig. 3a) also shows distinct trends in the three periods considered. In

205 2004-2007, we observe a relatively low calanoids abundance between km 110-150, ranging up to approximately 5 ind. L^{-1}. Downstream from km 110, we observe an increase in calanoids, resulting in a local maximum of calanoids of approximately 10 ind. L^{-1}, centered near km 90. In 2008-2014, the local maximum in calanoids abundance shifts in the upstream direction and increases. The overall calanoids abundance increases, with a maximum of approximately 17.5 ind. L^{-1} at km 110. In 2015-2018, the local maximum in calanoids abundance shifts further landwards to approximately km 140, with again a maximum of

210 approximately 17.5 ind. L^{-1}. We thus observe a land-inward shift and estuary-scale increase of the local calanoids abundance over time. However, the system-averaged, volume-weighted calanoids abundances are 4.9 ind. L^{-1}, 6.43 ind. L^{-1}, and 4.3 ind. L^{-1}, respectively, as the estuary is narrow and shallow in the upstream region. At the upstream boundary, non-calanoids are dominantly present (see Fig. 3b). On average, we observe an increase of the non-calanoids abundance in landward direction on the estuary scale in all three periods. As illustrated by the large standard error, the differences of the non-calanoids abundance

215 are not statistically significant between the three distinct periods.

3.1.2 Evolution in SPM and light extinction

Figure 4a shows the sub-surface time-averaged SPM concentration in the three periods considered. In all three periods, the SPM concentrations range up to approximately 150 mg L^{-1}. However, we observe significantly lower concentrations between approximately km 50-100 in 2004-2007. The lower SPM concentrations are especially visible between km 70-80, where we

220 observe concentrations below 50 mg L^{-1} in 2004-2007 and up to 150 mg L^{-1} after 2007. Moreover, in 2015-2018, we observe the largest SPM concentrations between km 80-120.

The light extinction coefficient shows a similar evolution to the SPM concentration (see Fig. 4b), with significantly lower values of approximately 4 m^{-1} between km 70-80 in 2004-2007 compared to the values of approximately 7 m^{-1} after 2007. However, although the average values are also higher between km 80-120 in 2015-2018, which is consistent with the SPM

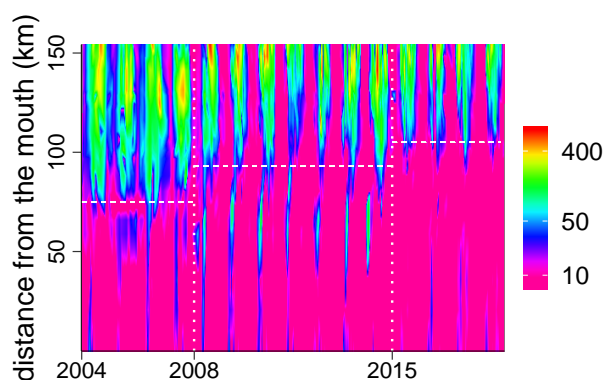225 observations, the differences are not statistically significant.

Figure 2. Observed Chl-a concentration (μg L^{-1}) in 2004-2018 and (b) the corresponding long-term time-averages of the Chl-a concentration and zooplankton abundance (i.e., calanoids abundance) in spring (Apr.-May). The error bars and shaded area depict the standard error of the Chl-a observations and zooplankton abundance, respectively. We observe a phytoplankton bloom in the brackish region (km 60-90) in spring in 2008-2014, which is absent in the other years considered. Simultaneously, we observe a land-inward shift of the zooplankton community.

(a) Time-averaged Chl-a concentration and calanoid abundance in spring

(b) Time-averaged Chl-a concentration and non-calanoid abundance in spring
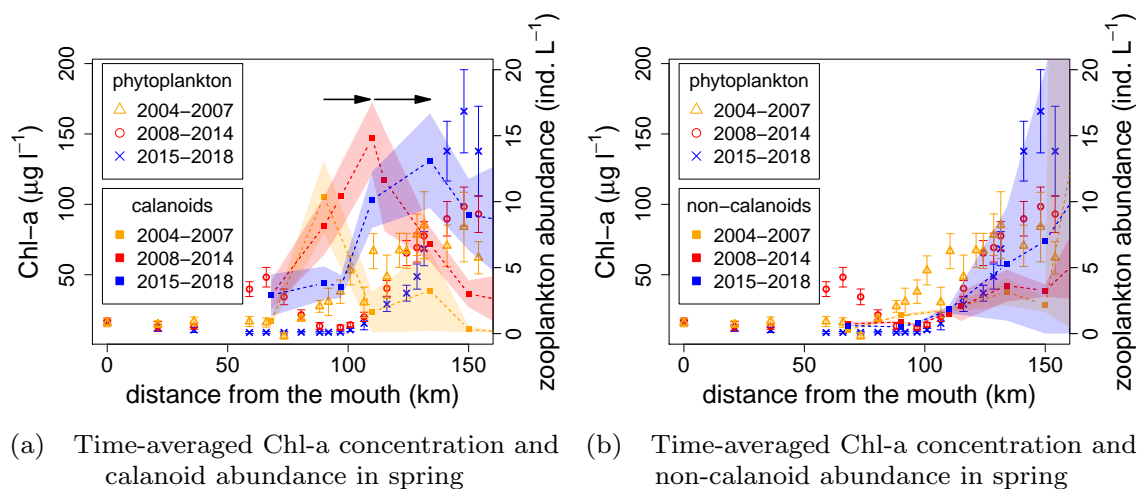
Figure 3. Long-term time-averages of the Chl-a concentration and (a) calanoids and (b) non-calanoids in spring (Apr.-May). The error bars and shaded area depict the standard error of the Chl-a observations and zooplankton abundance, respectively. We observe a phytoplankton bloom in the brackish region (km 60-90) in spring in 2008-2014, which is absent in the other years considered. Simultaneously, we observe a land-inward shift of the calanoids.

(a) Time-averaged SPM concentration in spring

(b) Time-averaged light-extinction coefficient in spring
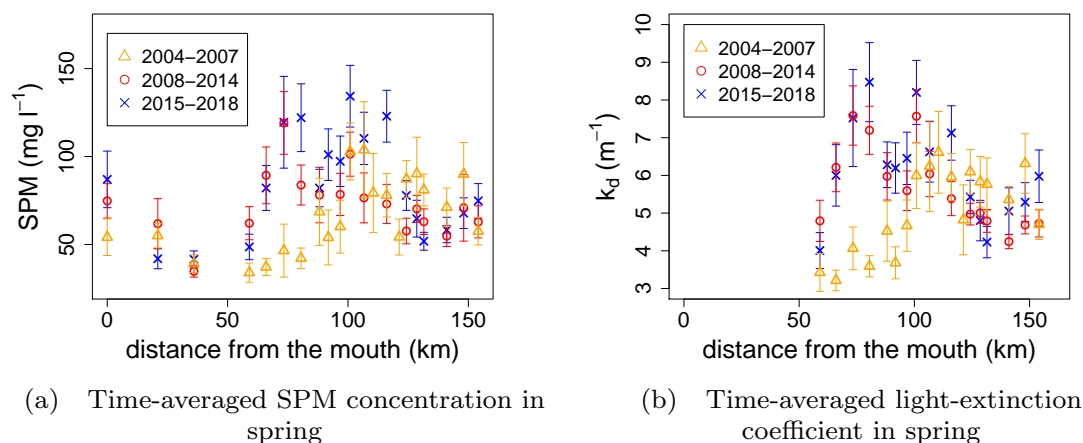
Figure 4. Long-term time-averaged observations in spring (Apr.-May) in 2004-2018 of (a) the water surface SPM concentration and (b) the light extinction coefficient k_d. The error bars depict the standard error of the observations.

3.1.3 Evolution in discharge and salinity intrusion

Figure 5a shows the long-term, monthly-averaged discharge in the three periods considered. In spring (Apr.-May), the average discharge is 85, 81, and 72 m^{-3} s^{-1} in 2004-2007, 2008-2014, and 2015-2018, respectively. We thus observe a slight decrease in total freshwater discharge over time.

Figure 5b shows the monthly-averaged salinity intrusion, which is defined as the distance from the mouth at which the salinity equals 2 ppt. We typically observe the opposite trend compared to the freshwater discharge: a larger discharge comes with a smaller salt intrusion. What is most important within the scope of this paper is the fact that in spring (Apr.-May) the salinity intrusion does not show major changes during the study period 2004-2018.

3.1.4 Evolution in photosynthetic parameters

Figure 6a shows the monthly- and system-averaged maximum photosynthetic rate μ_{max} in the three periods considered. In spring (Apr.-May), μ_{max} is approximately equal in 2004-2007 and 2008-2014, but significantly lower in 2015-2018. The corresponding time-averaged values are 6.59, 6.44, and 4.31 mg C (mg Chl-a)$^{-1}$ h^{-1}, respectively.

Figure 6b shows the monthly- and system-averaged photosynthetic efficiency α in 2004-2018. What is most important within the scope of this paper is that α is not significantly different in all three periods 2004-2007, 2008-2014, and 2015-2018 in spring. The corresponding time-averaged values are 0.0165, 0.0168, and 0.0188 mg C (mg Chl-a)$^{-1}$ h^{-1} [PAR]$^{-1}$, respectively.

(a) Time-averaged discharge
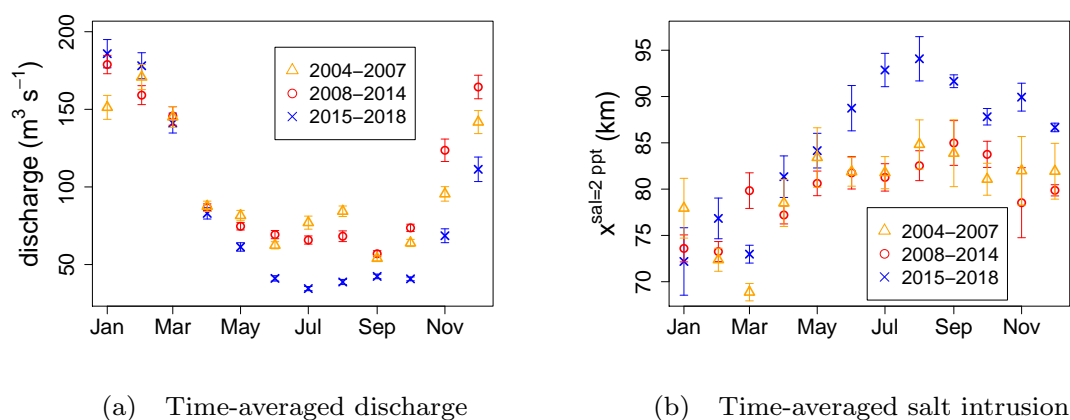

(b) Time-averaged salt intrusion

Figure 5. Long-term monthly-averaged observations in 2004-2018 of (a) the total freshwater discharge (at the upstream boundary and tributaries) and (b) the salinity intrusion defined as the distance at which the salinity equals 2 ppt. The error bars depict the standard error of the observations.
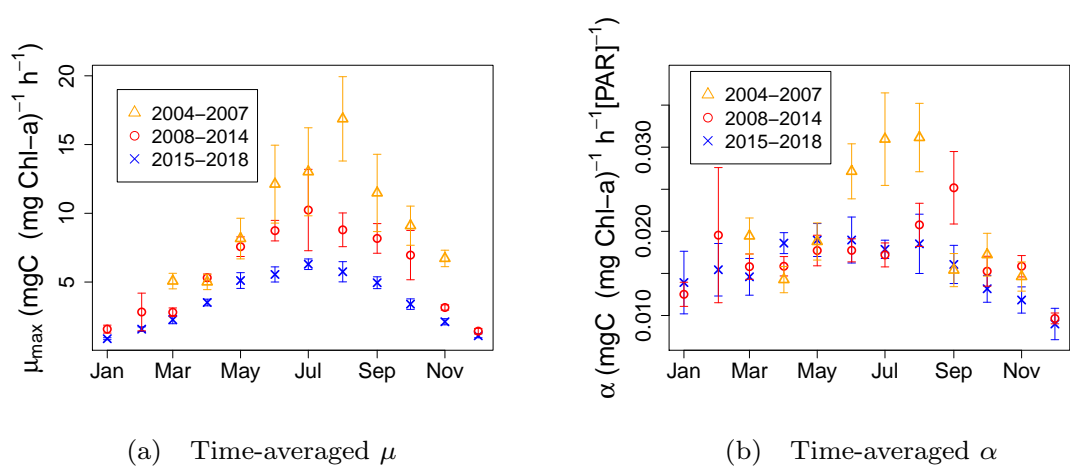

(a) Time-averaged μ

(b) Time-averaged α

Figure 6. Long-term monthly-averaged observations in 2004-2018 of the photosynthetic parameters (a) μ_{max} and (b) α. The error bars depict the standard error of the observations.

To conclude, long-term observations in the Scheldt estuary show an estuary-scale evolution in zooplankton abundance, SPM (cf. light extinction), $\mu_{\max}$, and, to a minor extend, in the freshwater discharge in the Scheldt estuary in 2004-2018 in spring. The determination of the changes in the observations that are responsible for the evolution in Chl-a concentration is difficult
245   based on the observations alone. Therefore, we apply a complementary model approach in the following section.

3.2   Evolution of Chl-a explained using model experiments

To quantify the impact of the observed trends presented in the previous section and alterations of other factors affecting phytoplankton growth on the Chl-a concentration, we calibrate our model and apply an extensive model sensitivity analysis.

3.2.1   Evolution in Chl-a and mortality rate (cf. zooplankton)

250   We calibrate the system-constant mortality rate m_0 and the influx of phytoplankton at the upstream boundary QP to the observed long-term time-averaged Chl-a concentrations separately for the three periods considered by minimizing our prescribed cost function. This results in an optimal parameter set $m_0 = 2.64 \times 10^{-6}$ s^{-1}, $QP = 2.46$ g s^{-1}, $m_0 = 1.19 \times 10^{-6}$ s^{-1}, $QP = 1.81$ g s^{-1}, and $m_0 = 0.83 \times 10^{-6}$ s^{-1}, $QP = 1.48$ g s^{-1}, in 2004-2007, 2008-2014, and 2015-2018, respectively.

Figures 7a-c show the corresponding modeled Chl-a concentration for the optimal choice of m_0 and QP in 2004-2007, 2008-
255   2014, and 2015-2018, respectively. The model captures the main features of the Chl-a distribution in 2004-2007. In 2008-2014, the model does not capture the accumulation of Chl-a in the brackish region, but does capture the Chl-a concentrations at the other locations. In 2015-2018, the model captures the main features of the Chl-a distribution, which is relatively simple: Chl-a flows into the Scheldt estuary at the upstream boundary and the Chl-a concentration decreases relatively fast in the downstream direction. Here, it is important to note that the observed Chl-a values between km 50 and 100 are below the detection limit of
260   10 μg L^{-1} and all modeled Chl-a concentrations lower than this limit are considered as 'good' by the cost function.

To conclude, the calibrated system-constant mortality rate seems to have increased after 2015. Simultaneously, our calibration shows a long term decrease in influx of phytoplankton QP at the upstream boundary. The model captures the main trends in the 2004-2007 and 2015-2018 case. However, the model does not capture the observed accumulation of Chl-a in the brackish region in 2008-2014 and thus the calibrated parameters in 2008-2014 should be taken with care. To further investigate
265   this accumulation of Chl-a and determine potential parameter values which may result in accumulation of Chl-a in the brackish region, we apply a sensitivity analysis in the following section.

3.2.2   Sensitivity study of model parameters

Figure 8a shows the sensitivity of the depth-averaged Chl-a concentration to the mortality rate m_0 in 2008-2014. At low $m_0 \lesssim 0.4 \times 10^{-6}$ s^{-1}, accumulation of Chl-a occurs in the brackish region, but also results in a significant increase in Chl-a
270   upstream from km 100, which is not observed.

Figure 8b shows the impact of variations in the sediment-induced light extinction coefficient k_c on the Chl-a model result, keeping other parameters at their default values. We have to decrease k_c by a factor of approximately 4 to obtain accumulation

(a)   Model and observed Chl-a concentration
in 2004-2007

(b)   Model and observed Chl-a concentration
in 2008-2014

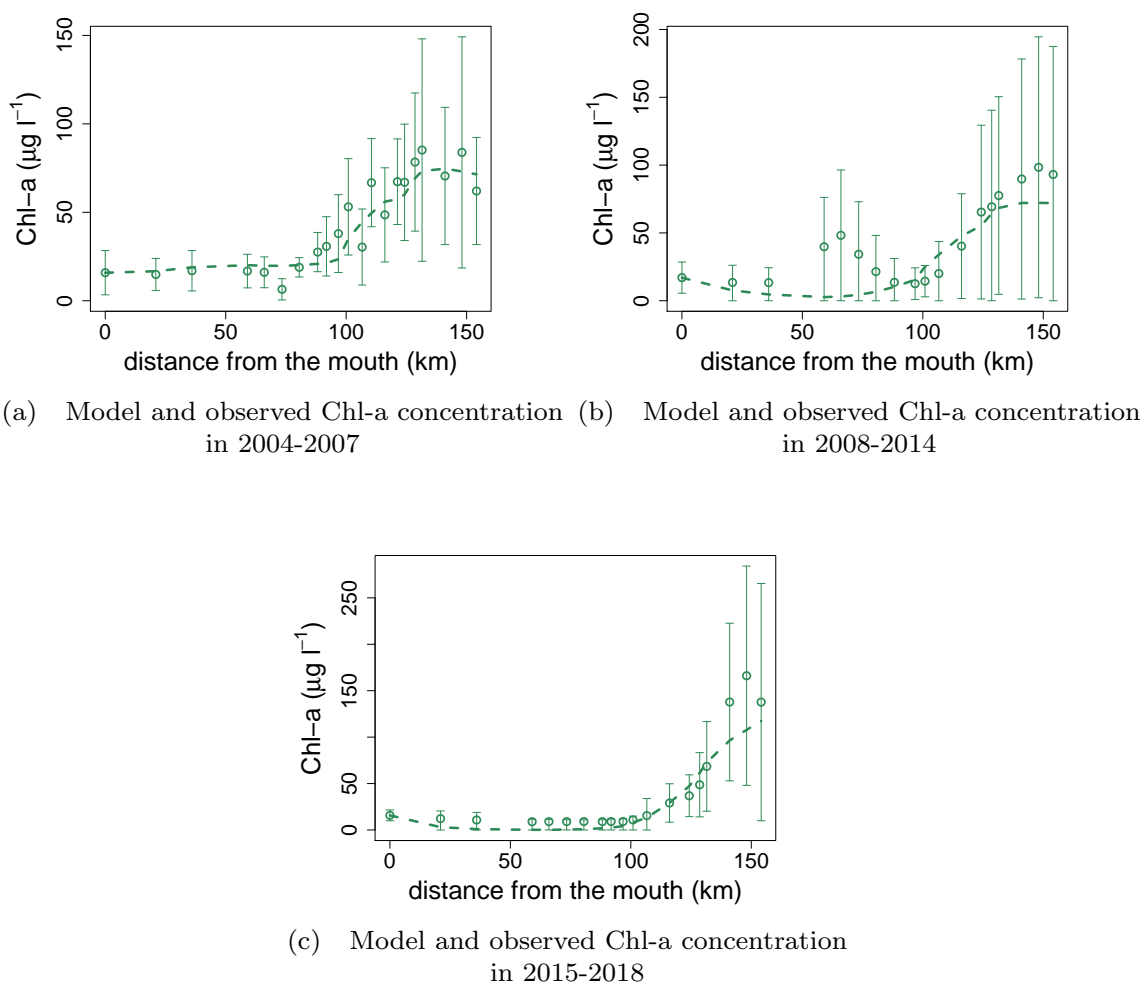(c)   Model and observed Chl-a concentration
in 2015-2018

Figure 7. Long-term time-averaged Chl-a observations (dots) and depth-averaged model result (dashed line) in spring (Apr.-May) in (a) 2004-2007, (b) 2008-2014, and (c) 2015-2018. The optimal (m_0,QP) pairs are $m_0 = 0.83 \times 10^{-6}$ s^{-1}, $QP = 1.48$ g s^{-1}, $m_0 = 1.19 \times 10^{-6}$ s^{-1}, $QP = 1.81$ g s^{-1}, and $m_0 = 2.64 \times 10^{-6}$ s^{-1}, $QP = 2.46$ g s^{-1}, respectively.
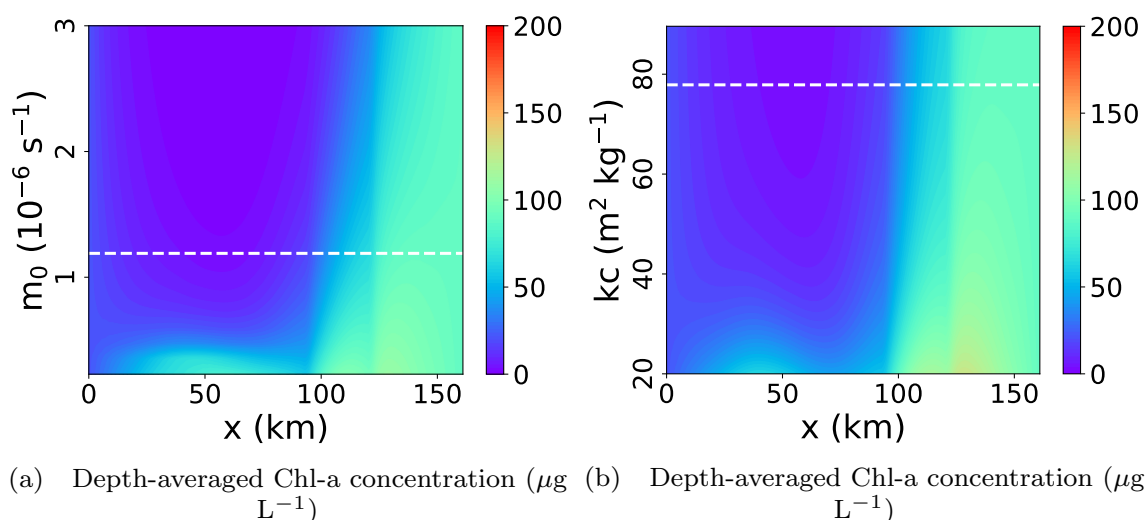
Figure 8. Sensitivity study of the depth-averaged Chl-a concentration in 2008-2014 to the (a) mortality rate m_0 and (b) the sediment-induced light extinction coefficient k_c. The parameter values of the reference case are depicted by the dashed horizontal lines.

of Chl-a in the brackish region. This difference is significantly larger than the variability that follows from the observations, which is between approximately 65 and 80 m^2 kg^{-1} (see Appendix D).

275   Figures 9a-9d show the sensitivity of the depth-averaged Chl-a concentration to the freshwater discharge Q, the maximum photosynthetic rate μ_{00} at 0 °C, the influx of Chl-a at the upstream boundary QP, and the Chl-a concentration at the seaside boundary P_{sea} in 2008-2014, again keeping the other variables at their default values. Changes in these parameters lead to changes in the upstream or downstream Chl-a concentration, but do not result in the accumulation of Chl-a in the brackish region. Therefore, changes in these parameters alone cannot explain the disappearance of accumulation of Chl-a in the brackish

280   region.

3.2.3   Chl-a distribution using parameter values that result in accumulation of Chl-a in the brackish region

Our sensitivity study shows that variability in the mortality rate m_0 and the sediment-induced light extinction coefficient k_c may result in accumulation of Chl-a in the brackish region in 2008-2014, while changes in the other parameters do not. To further analyze the impact of an adjustment of these two parameters on the Chl-a distribution, we calibrate these two parameters

285   to the Chl-a concentration in the brackish region in 2008-2014 only and present the resulting Chl-a distribution. Because we are interested in the individual impact of an adjustment of m_0 and k_c on the Chl-a distribution, we keep all other parameters fixed to the values used in the reference case presented in Fig. 7. Finally, we use the optimal parameter values of m_0 and k_c that result in accumulation of Chl-a in the brackish region in 2008-2014 in the other periods considered (i.e., 2004-2007 and 2015-2015) and show the corresponding impact on the Chl-a distribution.
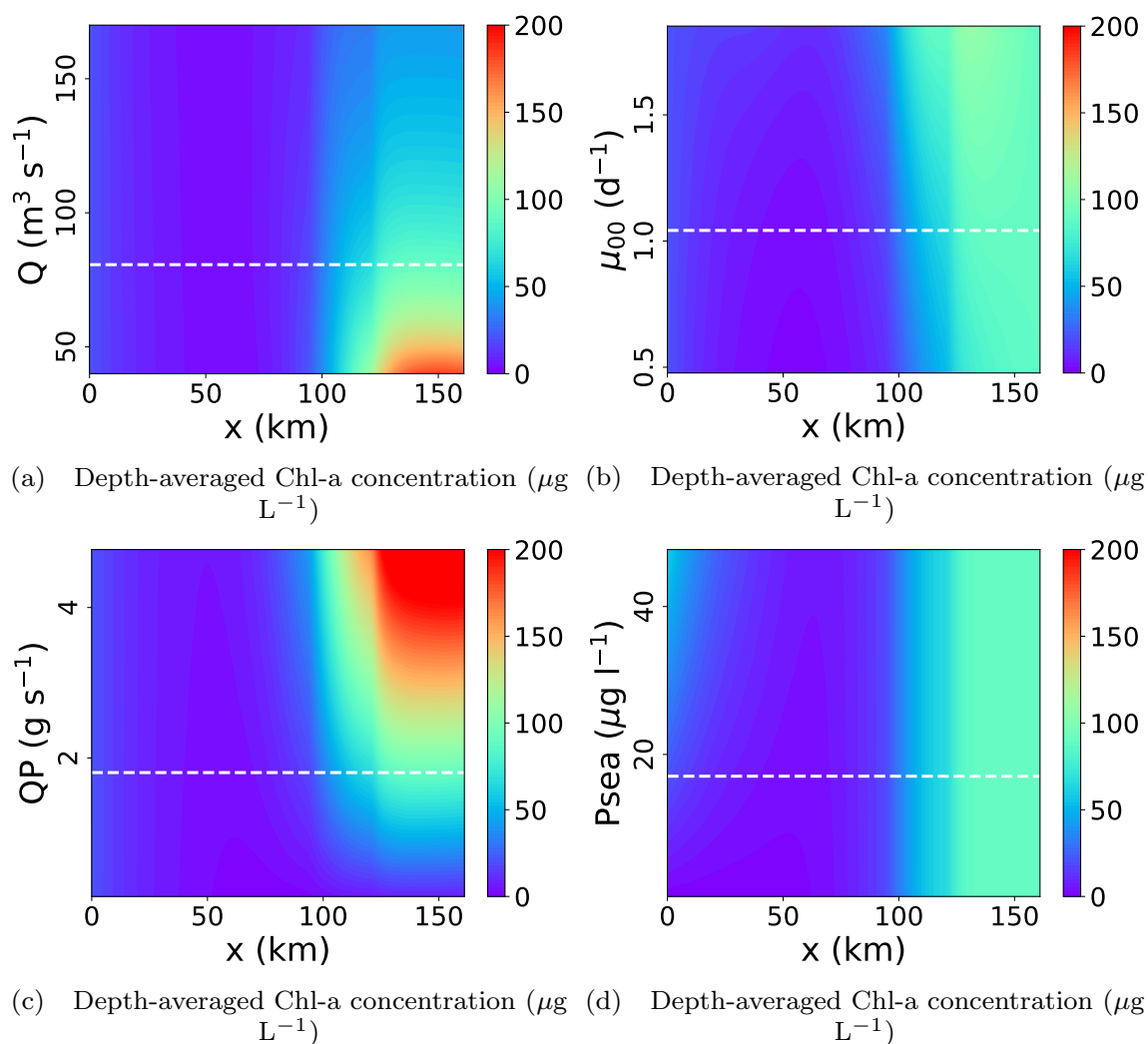
Biogeosciences
Discussions

Open Access

(a) Depth-averaged Chl-a concentration (μg L^{-1})

(b) Depth-averaged Chl-a concentration (μg L^{-1})

(c) Depth-averaged Chl-a concentration (μg L^{-1})

(d) Depth-averaged Chl-a concentration (μg L^{-1})

Figure 9. Sensitivity study of the depth-averaged Chl-a concentration in 2008-2014 to the (a) the total freshwater discharge Q, (b) the photosynthetic rate μ_{00} at 0 $^\circ$C, (c) the phytoplankton influx at the upstream boundary QP, and (d) the Chl-a concentration at the seaside boundary P_{sea}. The parameter values of the reference case are depicted by the dashed horizontal lines.

290   Calibration of the mortality rate m_0 and the sediment-induced light extinction coefficient k_c separately to the brackish Chl-a observations only (km 50-90) in 2008-2014 results in $m_{new} = 0.35 \times 10^{-6}$ s^{-1} and $k_c = 22.4$ m^2 kg^{-1}.

Figure 10b shows the corresponding modeled Chl-a distribution using this optimal m_{new} value. We also show the reference model result (ref. in Fig. 7b) when using the optimal $m_0 = 1.19 \times 10^{-6}$ s^{-1} calibrated to the Chl-a observations covering the full estuary. The recalibrated model results of Chl-a to the brackish region capture the magnitude of the Chl-a concentrations

295   in this region between km 50-90. However, this choice of m_{new} results in an overestimation of the Chl-a concentration near km 100 and downstream from km 50. This overestimation increases when we use the recalibrated m_{new} value in the other periods considered. In 2004-2007, the recalibrated model results (i.e., m_{new} in Fig. 10a) overestimates the Chl-a concentration in almost the entire estuary, in particular in the brackish region, which is mainly due to the significantly lower SPM concentrations in this region (see Fig. 4a). In 2015-2018, using m_{new} also results in an overestimation of the Chl-a concentrations (m_{new} in Fig.

300   10c).

When we recalibrate k_c to the brackish region only in 2008-2014, we again capture the magnitude of the Chl-a concentrations in the region between km 50-90 (k_c Figure 10b) and overestimate the Chl-a concentration near km 100 and downstream from km 50. Using this recalibrated k_c value, we again overestimate the Chl-a concentration in 2004-2007. In 2015-2018, recalibration of k_c has no major impact on the Chl-a distribution (k_c in Fig. 10c).

305   **3.2.4   Spatial variability in mortality rate due to grazing**

Although the recalibrated mortality rate captured the accumulation of Chl-a in the brackish region in 2008-2014, it results in an overestimation of Chl-a in both the downstream and upstream region. Furthermore, using this recalibrated mortality rate m_{new} in 2004-2007 and 2015-2018 results in a estuary-scale overestimation of the Chl-a concentration, again indicating that we have to use a different mortality rate for the three periods considered. This is our motivation to introduce spatial variability

310   in m by assuming a linear relationship between m and the calanoid and non-calanoid zooplankton abundance $Z^{calanoids}(x)$ and $Z^{non\text{-}calanoids}(x)$ [see Eq. (3)], with the corresponding linear scaling factors being defined as the grazing efficiencies g_1, and g_2, respectively. We estimate $Z^{calanoids}(x)$ and $Z^{non\text{-}calanoids}(x)$ as the (linearly interpolated) zooplankton abundance (i.e., the dashed curves in Figs. 3a-b, respectively) in which we extrapolate the zooplankton abundance in the downstream region where we do not have observations using the system-averaged abundance.

315   Calibration of g_1 and g_2 to the Chl-a observations in 2004-2007 and 2015-2018, and the Chl-a observations in the brackish region only in 2008-2014 results in the modeled Chl-a concentrations ($m_{spatial}$) presented in Figs. 10a, 10c, and 10b, respectively. In 2004-2007, a spatially varying m ($g_1 = 1.6$ and $g_2 = 0.93 \times 10^{-7}$ s^{-1} L) partly resolves the overestimation of the Chl-a in the brackish region and captures the local decrease in this region. However, more upstream at km 90, the Chl-a concentrations are slightly underestimated. In 2008-2014, although the Chl-a concentrations are slightly overestimated near km

320   100, the local increase in m ($g_1 = 0.24$ and $g_2 = 0.63 \times 10^{-7}$ s^{-1} L) significantly reduces the Chl-a concentrations and results in a local minimum of Chl-a near km 100, which complies with the observations. If we were to choose the calibrated values corresponding to 2004-2007 in 2008-2014, we would obtain a Chl-a distribution very similar to the reference case and we would thus not capture the accumulation of Chl-a in the brackish region (not shown). If we were to consider only the calanoids
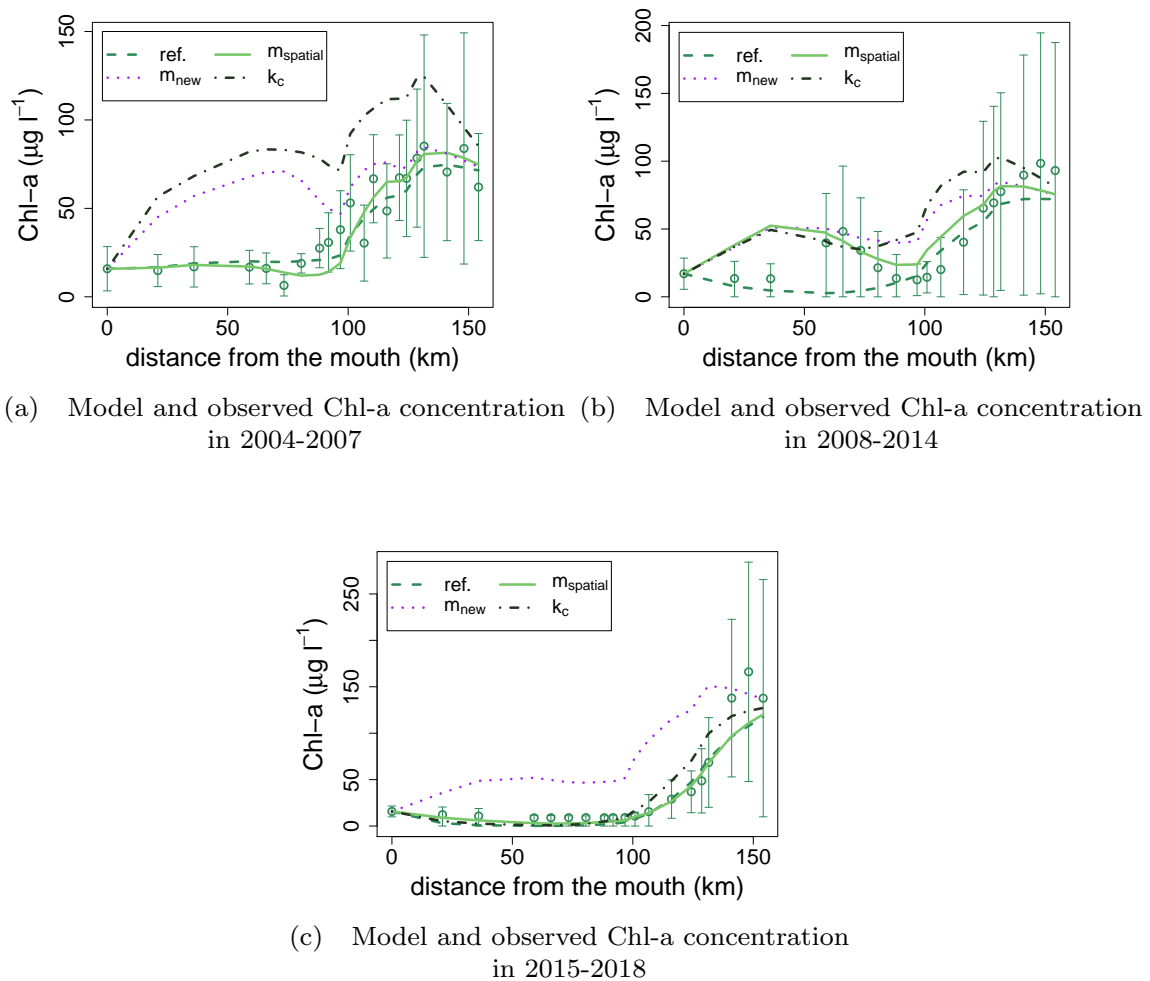
(a) Model and observed Chl-a concentration in 2004-2007

(b) Model and observed Chl-a concentration in 2008-2014

(c) Model and observed Chl-a concentration in 2015-2018

Figure 10. Long-term time-averaged Chl-a observations (dots) and depth-averaged model result (dashed line) in spring (Apr.-May) in (a) 2004-2007, (b) 2008-2014, and (c) 2015-2018. The optimal parameter values from Section 3.2.1 are used in the reference model result (ref.). We also show the model result in which we calibrated m_0 and k_c to the Chl-a observations in the brackish region in 2008-2014 only (m_{new} and k_c, respectively) and the model result in which we used a spatially varying mortality rate ($m_{spatial}$).

(so a reduction of one calibration parameter), we would not obtain the clear local minimum in Chl-a near km 100 (not shown).

325 We thus require an evolution in g_1 and g_2 to capture the accumulation of Chl-a in the brackish region. In 2015-2018, a spatially varying m ($g_1 = 1.6$ and $g_2 = 0.93 \times 10^{-7}$ s^{-1} L) has no major impact on the model results and results in a good correspondence between model and observations. We can thus capture the Chl-a distribution using the g_1 and g_2 values of 2004-2007. Finally, using the g_1 and g_2 values corresponding to 2008-2014 in 2015-2018 results in a system-scale overestimation of Chl-a (not shown).

330 To conclude, the sensitivity analysis of m_0 shows that accumulation in the brackish region is possible at low m_0. However, this results in an overestimation of the Chl-a concentrations downstream from km 50 and near km 100. The latter can partly be resolved by considering spatial variability in the morality rate m, which we based on the zooplankton observations and thus suggests that the evolution in the zooplankton abundance in the Scheldt estuary may partly explain the evolution in the Chl-a distribution in spring. Here, we require different g_1 and g_2 values in 2008-2014. In 2004-2007 and 2015-2018, we capture

335 the Chl-a distribution on the estuary-scale using similar g_1 and g_2. The reason for this evolution in g_1 and g_2 is unclear and discussed in the following section.

4   Discussion

In this section, we first discuss the observations and model results. Next, we combine all results to explain the long-term evolution of the estuary-scale Chl-a concentrations.

340 ### 4.1   Suggested importance of grazing

To explain the temporary occurrence of accumulation of Chl-a in the brackish region in 2008-2014, we studied long-term observations of the factors affection phytoplankton growth and carried out an extensive model sensitivity analysis. The complementary model approach allowed us to detect causalities instead of correlations and quantitatively determine which processes are essential to capture the long-term evolution in Chl-a concentrations on the estuary-scale. Our results suggest that a change

345 in mortality rate is the main factor to explain the appearance and disappearance of Chl-a accumulation in the brackish region and that other parameters (e.g., SPM) alone cannot explain this observed evolution in Chl-a.

Mortality rate results from a complex interaction between physical-bio-chemical processes. Important indicators impacting the mortality rate are viruses (Brussaard, 2004), phytoplankton community competition (Beckett and Weitz, 2017), salinity stress (Lionard et al., 2005b), and nutrient loads. Given the favorable nutrient concentrations for phytoplankton growth in the

350 Scheldt estuary between 2004-2018 (Maris and Meire, 2017), we do not expect that nutrients are important. Moreover, we did not observe major changes in salinity (see Fig. A1) in the brackish region in spring over the last decade. This suggests that the change in mortality rate is caused by other factors such as viruses, phytoplankton community composition, and grazing.

Without specific evidence of changes in viruses or planktonic community, we hypothesize that changes in grazing of phytoplankton is the core reason for the long-term changes in the mortality rate. This idea is supported by the long-term land-inward

355 shift of the phytoplankton grazers and our model approach, which showed an improvement of the model results when making

the mortality rate dependent on the zooplankton abundance. Moreover, a dominant impact of zooplankton grazing on the mortality rate complies with Calbet and Landry (2004) who studied 136 estuarine systems and showed that zooplankton grazes on average approximately 60 % of the primary production. Moreover, by comparing Chl-a concentrations and biomass concentrations of the *E. affinis*-dominated zooplankton population in the St Lawrence estuary (Canada), Winkler et al. (2003) showed
360   that *E. affinis* is likely to be a major cause of the downstream decrease in Chl-a concentration.

The values and range of the mortality rate and grazing efficiency found by our model comply with the literature. Assuming a system-constant mortality rate, we found mortality rate values ranging from $0.83 - 2.64 \times 10^{-6}$ s^{-1}, which complies with the value of approximately 1.1×10^{-6} s^{-1} presented in Desmit et al. (2005) who studied a real-case in the Scheldt estuary near km 115. Incubation experiments carried out with adult *E. Affinis* around km 80 in the Scheldt estuary during spring 2013 and
365   2014 show g values between 1.54×10^{-8} and 2.78×10^{-6} s^{-1} L (Chambord et al., in prep.), overlapping with the modeled values in this study. Also, the fact that we obtained a different grazing efficiency for the three distinct periods is not surprising because the translation of zooplankton abundance to grazing and mortality rates is complex; it does not only depend on the zooplankton community (Hoffman et al., 2008) and its inter-specie predation (Soto and Hurlbert, 1991), but is also influenced by both biotic and abiotic factors. For example, higher SPM concentrations may impact selective feeding (Tackx et al., 2003)
370   and thereby decrease the grazing efficiency. Additionally, Mialet et al. (2011) suggested that variability in phytoplankton size in the Scheldt estuary (Muylaert and Sabbe, 1999) may influence the feeding efficiency of the copepod *Eurytemora affinis*.

4.2   Hypothesized schematic reconstruction of the estuary-scale Chl-a concentrations

In this section, we combine all results into a schematic reconstruction of the long-term evolution in Chl-a concentrations. To do so, we add observations of two crucial variables that impact the zooplankton abundance: the oxygen concentration and
375   fish abundance. Figure 11 shows the long-term trends resulting from the OMES observations in spring. The fish abundance follows from visual inspection of the figures showing the fish abundance in spring presented in Breine et al. (2018). The grazing efficiency is the grazing efficiency corresponding to calanoids [which dominate the brackish region (km 60-90) in spring] and follows from the calibration of g_1 carried out in Section 3.2.2. Note that Fig. 11 and the reasoning below is supported by observations but still needs to be verified by a model that explicitly resolves zooplankton dynamics. As such, we present Fig.
380   11 as a hypothesis.

In 2004-2007, the growth conditions for phytoplankton in the brackish region seem to have been optimal (lowest SPM concentrations, see SPM brack. in Fig. 11). Zooplankton was abundant in the brackish region because the fish population was low (Breine et al., 2018). Zooplankton was limited to the brackish region because the oxygen concentrations in the freshwater region were too low (< 4 mg L^{-1}) to allow for the occurrence of the dominant calanoid species *Eurytemora affinis* (Appeltans,
385   2003; Mialet et al., 2010, 2011). The environmental conditions (e.g., low SPM) resulted in a high grazing efficiency. The combination of this large grazing efficiency and a high zooplankton abundance in the brackish region hindered accumulation of Chl-a in this region significantly because of a top down control by zooplankton (see phyto. brack. in Fig. 11).

In 2007-2014, growth conditions changed in the brackish region. On the one hand, there was a significant increase in SPM. On the other hand, the implementation of the wastewater treatment capacity in, for example, Brussels in 2006 (Brion et al.,
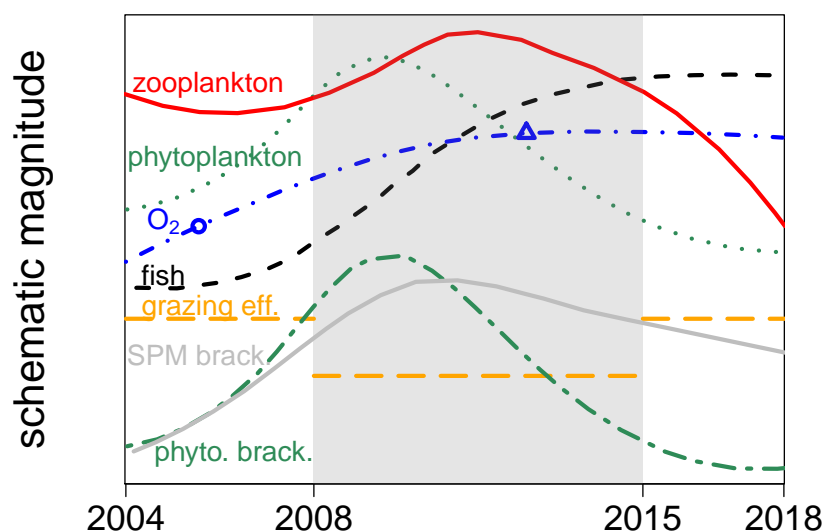
Figure 11. Schematic evolution of the volume-weighted phytoplankton concentration (phytoplankton), volume-weighted zooplankton abundance (zooplankton), estuarine fish abundance (fish), volume-weighted oxygen concentration (O_2), and (calibrated) grazing efficiency (grazing eff.) by calanoids in the Scheldt estuary and the volume-weighted phytoplankton abundance (phyto. brack.) and volume-weighted SPM concentration (SPM brack.) in the brackish region in spring (Apr.-May) in 2004-2018. The blue circle and triangle depict the critical oxygen concentration of 2.5 and 4 mg L^{-1}, respectively.

390   2015) resulted in a significant improvement of the water quality (Maris and Meire, 2017; Cox et al., 2019). In particular, the oxygen levels significantly increased and did not show critical concentrations for fish abundance below 2.5 mg L^{-1} (see O_2 in Fig. 11), resulting in a significant increase in estuarine fish population in spring after 2007 (Breine et al., 2018) (see fish in Fig. 11). These fish include juveniles of dominant fish species in the Scheldt estuary such as sprat and herring, of which the dominant calanoid *Eurytemora affinis* is an important food source (Maes et al., 2005). Moreover, mean oxygen values of ~ 4

395   mg L^{-1} in the freshwater region were observed, allowing for the occurrence of *Eurytemora affinis* in this region (Appeltans, 2003; Mialet et al., 2010, 2011; Chambord et al., 2016). The combined effect of an increase in fish population and an increase in oxygen concentrations in the freshwater region resulted in a land-inward shift and system-scale increase of zooplankton. In the brackish region, a change in environmental conditions (e.g., high SPM concentrations) decreased the grazing efficiency. Observations suggest that the balance of a deterioration of the light climate (i.e., increased SPM) and lowering of the grazing

400   pressure ultimately favored Chl-a growth in the brackish zone. More upstream, the land-inward shift of zooplankton resulted in a local minimum of Chl-a.

In 2015-2018, the growth conditions in the brackish region were apparently less optimal (decrease in $\mu_{\max}$) and the grazing efficiency seems to have increased. The reasons for this are not fully understood. The result was a disappearance of accumulation of Chl-a in the brackish region. A further increase in oxygen and fish population allowed the zooplankton population to

405   further shift land-inward, resulting in a rapid decrease of the Chl-a concentration in the downstream direction at the upstream boundary and a volume-weighted decrease of the zooplankton abundance.

5   Conclusions

In this paper, we studied the long-term estuary-scale evolution of the spring phytoplankton (cf. Chl-a) distribution in the Scheldt estuary. We focused on the appearance and disappearance of phytoplankton accumulation in the brackish region in spring in

410   2004-2018.

We first analyzed long-term in situ observations covering the full estuary of the SPM concentration, zooplankton abundance, and other variables affecting net phytoplankton growth, showing a long-term estuary-scale evolution in not only the SPM distribution and zooplankton abundance, but also in the freshwater discharge and maximum photosynthetic rate. Next, to detect the evolution in these variables that is essential to capture the evolution of phytoplankton, we employed a model approach

415   supported by the observations. Our model approach suggests that a change in mortality rate and grazing by zooplankton mainly explains the long-term estuary-scale evolution of phytoplankton in spring.

Although our model approach simplifies reality and shows (local) anomalies when comparing phytoplankton model results and observations, it allows us to quantitatively determine the importance of various factors affecting phytoplankton growth on the estuary-scale. This knowledge is important for moving forward using more complex numerically costly models. Our results

420   highlight the importance of insight into the zooplankton dynamics to understand the phytoplankton dynamics in the Scheldt estuary. Further research is required to determine the mechanisms that may have caused these long-term estuary-scale changes in mortality rate and grazing.

Appendix A: Salinity profile

Following Warner et al. (2005), we fit the salinity data measured in spring in the Scheldt estuary to the following postulated

425   salinity distribution:

$$\frac{s_{\mathrm{sea}}}{2}\left(1 - \tanh\frac{x - x_c^{\mathrm{Sal.}}}{x_L^{\mathrm{Sal.}}}\right), \tag{A1}$$

where s_{sea} is the salinity boundary condition at the mouth and $x_c^{\mathrm{Sal.}}$ and $x_L^{\mathrm{Sal.}}$ are further undefined calibration parameters. Figure A1 shows the salinity data and corresponding data fit in spring for the three periods considered. The corresponding parameter values are listed in the Supporting Information attached to this paper.
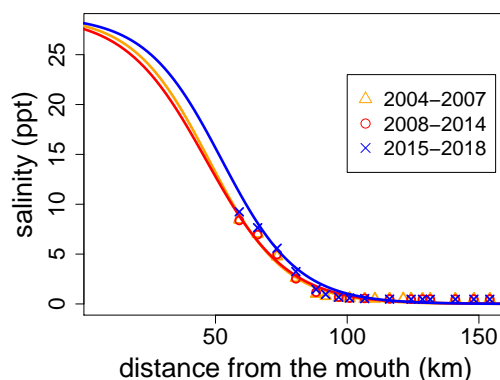
22

Figure A1. Measured salinity in the Scheldt estuary in spring and the corresponding data fit using Eq. (A1).

430 **Appendix B: Temperature dependence of μ_{max}**

Following Eppley (1972), we postulate the following temperature dependence of the maximum growth rate $\mu_{\mathrm{max}}(T)$:

$$\mu_{\mathrm{max}}(T) = \mu_{00} \cdot \mu_{01}^{T}, \tag{B1}$$

in which T is the water temperature and μ_{00} and μ_{01} are calibration parameters. Figure B1a shows the long-term averaged temperature dependence in 2004-2018. Figure B1b shows the μ_{max}-T plot for the 2015-2018 reference case and the corresponding

435 data fit following Eq. (B1), resulting in $\mu_{00} = 1.00 \times 10^{-5}$ s^{-1} and $\mu_{01} = 1.05$. Similarly, we have $\mu_{00} = 1.21 \times 10^{-5}$ s^{-1} and $\mu_{01} = 1.07$ and $\mu_{00} = 1.12 \times 10^{-5}$ s^{-1} and $\mu_{01} = 1.10$ in 2008-2014 and 2004-2007, respectively.

Appendix C: SPM distribution

Following Horemans et al. (2020a), we calibrate the erosion and flocculation characteristics by calibrating the residual SPM model output to the corresponding long-term residual SPM observations in 2015-2018 (see Fig. C1a). The corresponding

440 model parameters are the erosion parameter M and λ, which determines the strength of the flocs. The optimal values are $\lambda = 65.9 \times 10^{-6}$ s$^{-1/2}$ m^2 and $M = 4 \times 10^{-3}$ s m^{-1}.

As reasoned by Brouwer et al. (2018), Dijkstra et al. (2019b), and Horemans et al. (2020a), between km 70-80 we have an increase in SPM due to dumping and dredging activities. However, this is not included in model because the dredging and dumping activities act on a much smaller temporal scale ($\sim$ hours) and can thus be considered as a background SPM

445 concentration, whereas our model computes the long-term SPM distribution. To guaranty that we capture the magnitude of the observed SPM concentrations at the dredging and dumping location, we add a background SPM concentration originated by dredging and dumping activities to our model results. More specifically, we replace the model concentration by the (smoothed)
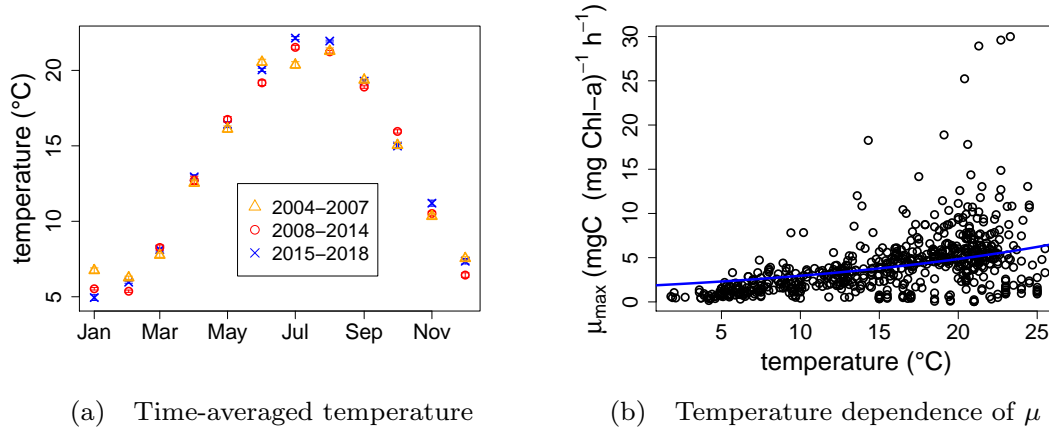
(a)   Time-averaged temperature

(b)   Temperature dependence of μ

Figure B1. (a) Long-term time-averaged temperature observations between 2004-2018. (b) $\mu_{\max}$-T plot for the 2015-2018 reference case and the corresponding data fit using Eq. (B1), resulting in $\mu_{00} = 1.00 \times 10^{-5}$ s^{-1} and $\mu_{01} = 1.05$.

SPM observations between km 70 and 80 and beyond km 125. The resulting modeled SPM distribution is presented in Fig. C1b.

450   To estimate the sensitivity of phytoplankton growth to the SPM concentration, we estimate the SPM distribution between 2004-2007 and 2008-2014 for which we only have water surface SPM observations. To this end, we first divide the water surface SPM concentration observed in 2004-2007 and 2008-2014 by the observations between 2015-2018 (see Fig. 4a). The resulting (interpolated) ratios are presented in Figs. C2a and C2b, respectively. Next, we use these ratios to scale the profiles of the modeled SPM concentrations in 2015-2018, thus keeping the shape of the vertical profiles the same. This results in the

455   estimated modeled SPM distribution in 2004-2007 and 2008-2014 presented in Figs. C1c and C1d, respectively.

Appendix D: Sediment-induced light extinction coefficient

Within the OMES campaign, the exponential light extinction coefficient k_d is computed by measuring the solar irradiance at the water surface E_0 and the light intensity at a depth d of approximately 1 m. Neglecting background and phytoplankton-induced light extinction, we can compute the sediment-induced light extinction k_c as

460   $$k_d d = k_c \int_0^d c(z', t) dz',$$ (D1)

Biogeosciences
Discussions

(a)   Observed SPM concentration in
2015-2018

(b)   Modeled SPM concentration in
2015-2018

(c)   Modeled SPM concentration in
2004-2007

(d)   Modeled SPM concentration in
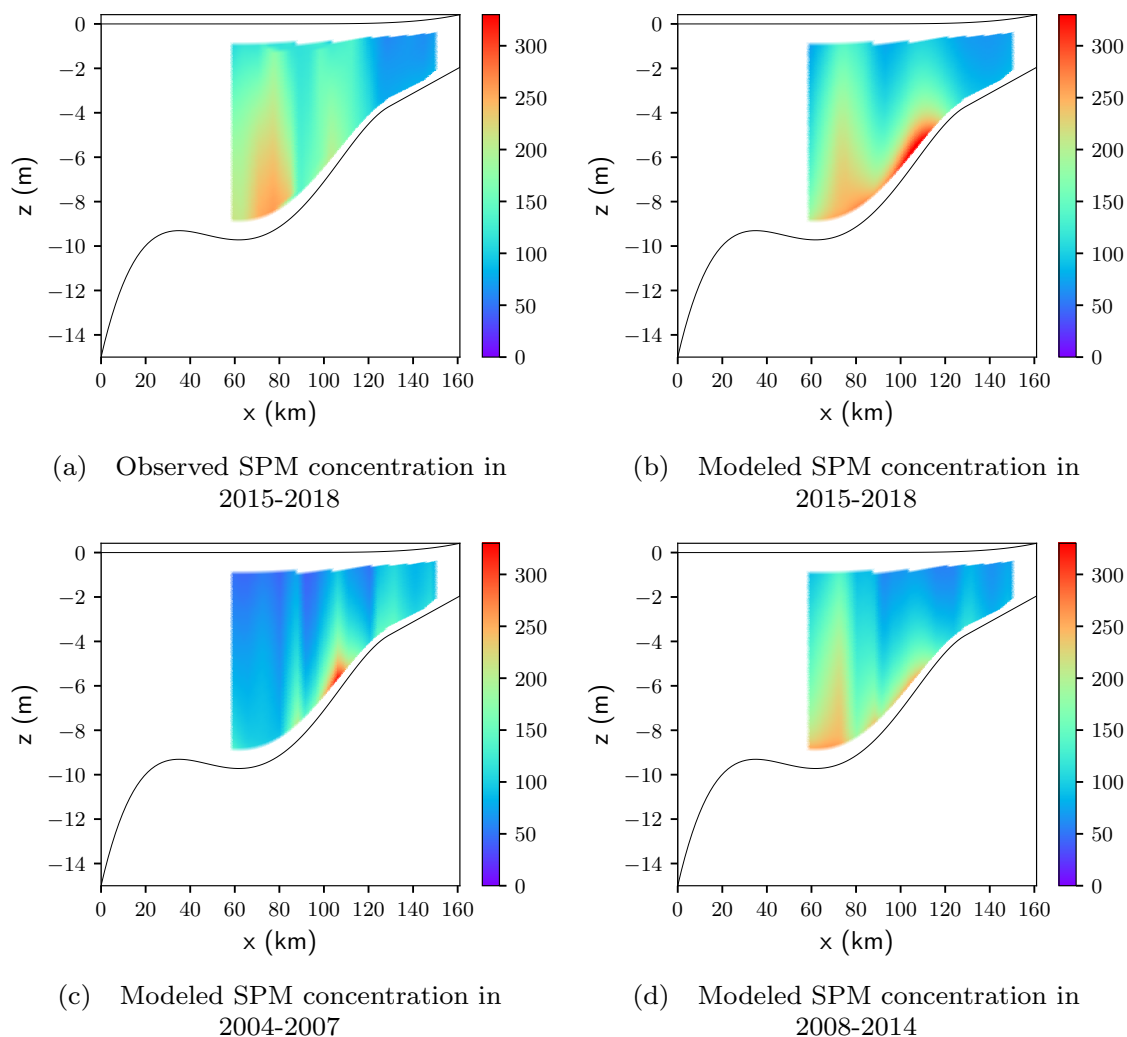2008-2014

Figure C1. (a) The long-term time-averaged observations and (b) the modeled SPM concentration in spring 2015-2018. (c)-(d) Modeled SPM concentrations which follows from scaling the vertical profiles of presented in (a). The scaling is quantified by computing the ratio of the observed surface SPM concentrations of the various periods.

(a)   SPM ratio in 2004-2007

(b)   SPM ratio in 2008-2014
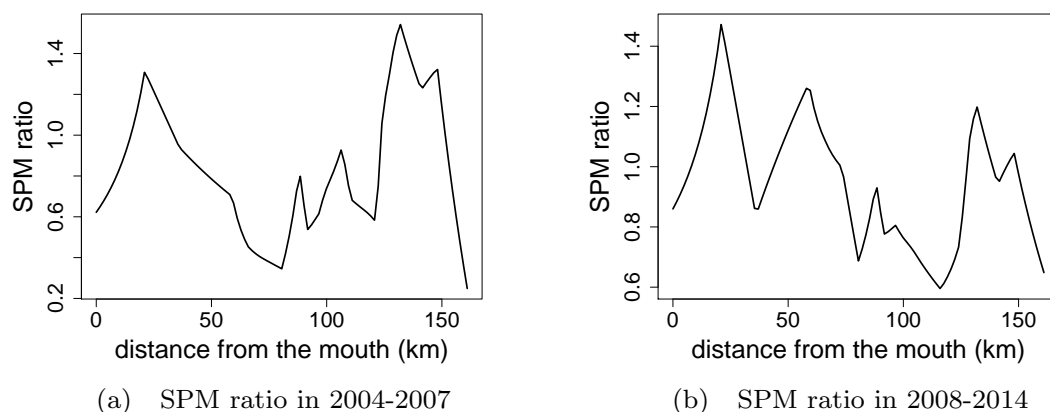
Figure C2. The (interpolated) water surface SPM observations divided by the observations in 2015-2018 between (a) 2004-2007 and (b) 2008-2014.

in which z' is the water depth and c is the modeled SPM concentration (see Fig. C1). Consequently, the time-averaged sediment-induced ligth extinction coefficient $\overline{k_c}$ can be approximated by

$$\overline{k_c} = \overline{\frac{k_d d}{\int_0^d c(z',t)dz'}},$$

$$\approx \frac{\overline{k_d d}}{\int_0^d c(z',t)dz'}, \tag{D2}$$

465   (D3)

which results in $k_c \approx 72$ m^2 kg^{-1} in 2015-2018 for $d = 1$ m. To quantify the impact of variability in the integration depth d on the estimated value of k_c, Fig. D1a shows the estimated k_c value as a function of d. If we assume a vertically constant sediment concentration, Eq. (D1) simplifies to the linear relationship $k_d = k_c c(t)$, which results in a slightly lower k_c value of approximately 68 m^2 kg^{-1}. The corresponding data fit for 2015-2018 is presented in Fig. D1b. Similarly, k_c approximates 78

470   m^2 kg^{-1} and 81 m^2 kg^{-1} in 2008-2014 and 2004-2007, respectively.

Code and data availability. The data presented in this paper in the Belgian and Dutch region of the Scheldt estuary is third party data and was accessed through http://www.omes-monitoring.be/en/data and https://waterinfo.rws.nl/, respectively. The iFlow version 2.9 code with the flocculation extension and an input file example are available through https://doi.org/10.5281/zenodo.4560637.

(a) Sediment-induced light extinction coefficient assuming a vertically non-constant SPM profile

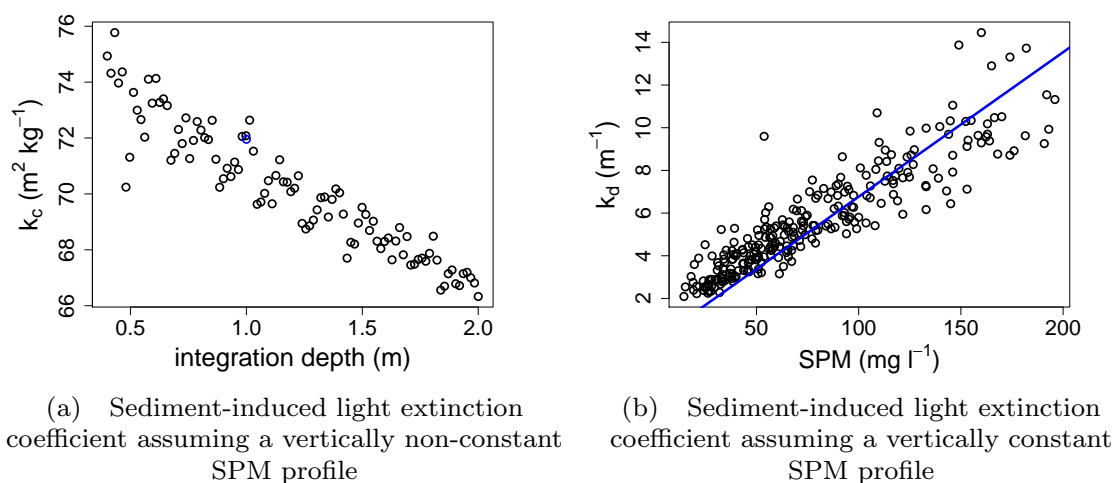(b) Sediment-induced light extinction coefficient assuming a vertically constant SPM profile

Figure D1. (a) Sediment-induced light extinction coefficient k_c in 2015-2018 for various integration depths d using Eq. (D2). Because the light extinction coefficient k_d is measured at approximately 1 m depth, we use the corresponding k_c value of 72 m^2 kg^{-1} in our model (depicted in blue). (b) Estimation of k_c in 2015-2018 assuming a vertically constant suspended sediment profile. By doing so, k_c equals the slope of the linear relationship between k_d and SPM (depicted by the blue line).

References

Alpine, A. E. and Cloern, J. E.: Trophic interactions and direct physical effects control phytoplankton biomass and production in an estuary, Limnology and Oceanography, 37, 946–955, https://doi.org/10.4319/lo.1992.37.5.0946, 1992.

Appeltans, W.: Zooplankton in the Schelde estuary (Belgium/The Netherlands). The distribution of Eurytemora affinis: effect of oxygen?, Journal of Plankton Research, 25, 1441–1445, https://doi.org/10.1093/plankt/fbg101, 2003.

Arndt, S., Lacroix, G., Gypens, N., Regnier, P., and Lancelot, C.: Nutrient dynamics and phytoplankton development along an estuary-coastal zone continuum: A model study, Journal of Marine Systems, 84, 49–66, https://doi.org/10.1016/j.jmarsys.2010.08.005, 2011.

Beckett, S. J. and Weitz, J. S.: Disentangling niche competition from grazing mortality in phytoplankton dilution experiments, PLOS ONE, 12, e0177517, https://doi.org/10.1371/journal.pone.0177517, 2017.

Breine, J., De Bruyn, A., Galle, L., Lambeens, I., Maes, Y., and Van Thuyne, G.: Monitoring van het visbestand in het Zeeschelde-estuarium.: Viscampagnes 2017, no. 40 in Rapporten van het Instituut voor Natuur- en Bosonderzoek, Instituut voor Natuur- en Bosonderzoek, België, https://doi.org/10.21436/inbor.14245903, 2018.

Brion, N., Verbanck, M. A., Bauwens, W., Elskens, M., Chen, M., and Servais, P.: Assessing the impacts of wastewater treatment implementation on the water quality of a small urban river over the past 40 years, Environmental Science and Pollution Research, 22, 12720–12736, https://doi.org/10.1007/s11356-015-4493-8, 2015.

Brouwer, R. L., Schramkowski, G. P., Dijkstra, Y. M., and Schuttelaars, H. M.: Time Evolution of Estuarine Turbidity Maxima in Well-Mixed, Tidally Dominated Estuaries: The Role of Availability- and Erosion-Limited Conditions, Journal of Physical Oceanography, 48, 1629–1650, https://doi.org/10.1175/JPO-D-17-0183.1, 2018.

Brussaard, C. P. D.: Viral Control of Phytoplankton Populations-a Review1, The Journal of Eukaryotic Microbiology, 51, 125–138, https://doi.org/10.1111/j.1550-7408.2004.tb00537.x, 2004.

Calbet, A. and Landry, M. R.: Phytoplankton growth, microzooplankton grazing, and carbon cycling in marine systems, Limnology and Oceanography, 49, 51–57, https://doi.org/10.4319/lo.2004.49.1.0051, 2004.

Chambord, S., Maris, T., Colas, F., Van Engeland, T., Sossou, A. C., Azémar, F., Le Coz, M., Cox, T., Buisson, L., Souissi, S., Meire, P., and Tackx, M.: Mesozooplankton affinities in a recovering freshwater estuary, Estuarine, Coastal and Shelf Science, 177, 47–59, https://doi.org/10.1016/j.ecss.2016.04.016, 2016.

Cira, E. K., Paerl, H. W., and Wetz, M. S.: Effects of Nitrogen Availability and Form on Phytoplankton Growth in a Eutrophied Estuary (Neuse River Estuary, NC, USA), PLOS ONE, 11, https://doi.org/10.1371/journal.pone.0160663, 2016.

Cox, T. J. S., Maris, T., Van Engeland, T., Soetaert, K., and Meire, P.: Critical transitions in suspended sediment dynamics in a temperate meso-tidal estuary, Scientific Reports, 9, 12745, https://doi.org/10.1038/s41598-019-48978-5, 2019.

Desmit, X., Vanderborght, J. P., Regnier, P., and Wollast, R.: Control of phytoplankton production by physical forcing in a strongly tidal, well-mixed estuary, Biogeosciences, 2, 205–218, https://doi.org/10.5194/bg-2-205-2005, 2005.

Dijkstra, Y. M., Brouwer, R. L., Schuttelaars, H. M., and Schramkowski, G. P.: The iFlow modelling framework v2.4: a modular idealized process-based model for flow and transport in estuaries, Geoscientific Model Development, 10, 2691–2713, https://doi.org/10.5194/gmd-10-2691-2017, 2017.

Dijkstra, Y. M., Chant, R. J., and Reinfelder, J. R.: Factors Controlling Seasonal Phytoplankton Dynamics in the Delaware River Estuary: an Idealized Model Study, Estuaries and Coasts, 42, 1839–1857, https://doi.org/10.1007/s12237-019-00612-3, 2019a.

Biogeosciences Open Access
Discussions
EGU

Dijkstra, Y. M., Schuttelaars, H. M., and Schramkowski, G. P.: Can the Scheldt River Estuary become hyperturbid? A model
525   analysis of suspended sediment concentrations and transport in response to channel deepening, Ocean Dynamics, 69, 809–827,
        https://doi.org/10.1007/s10236-019-01277-z, 2019b.

Eilers, P. H. C. and Peeters, J. C. H.: A Model for the Relationship Between Light-Intensity and the Rate of Photosynthesis in Phytoplankton,
        Ecological Modelling, 42, 199–215, https://doi.org/10.1016/0304-3800(88)90057-9, 1988.

Eppley, R. W.: Temperature and phytoplankton growth in the sea, Fish. bull, 70, 1063–1085, 1972.

530 Filardo, M. J. and Dunstan, W. M.: Hydrodynamic control of phytoplankton in low salinity waters of the James River estuary, Virginia,
        U.S.A., Estuarine, Coastal and Shelf Science, 21, 653–667, https://doi.org/10.1016/0272-7714(85)90064-2, 1985.

Garnier, J., Servais, P., Billen, G., Akopian, M., and Brion, N.: Lower Seine River and estuary (France) carbon and oxygen budgets during
        low flow, Estuaries, 24, 964–976, https://doi.org/10.2307/1353010, 2001.

Hoffman, J. C., Bronk, D. A., and Olney, J. E.: Organic matter sources supporting lower food web production in the tidal freshwater portion
535   of the York River estuary, Virginia, Estuaries and Coasts, 31, 898–911, https://doi.org/10.1007/s12237-008-9073-4, 2008.

Horemans, D. M. L., Dijkstra, Y. M., Schuttelaars, H. M., Meire, P., and Cox, T. J. S.: Unraveling the essential effects of floccu-
        lation on large-scale sediment transport patterns in a tide-dominated estuary, Journal of Physical Oceanography, 50, 1957–1981,
        https://doi.org/10.1175/jpo-d-19-0232.1, 2020a.

Horemans, D. M. L., Meire, P., and Cox, T. J. S.: The impact of temporal variability in light-climate on time-averaged primary production and
540   a phytoplankton bloom in a well-mixed estuary, Ecological Modelling, 436, 109 287, https://doi.org/10.1016/j.ecolmodel.2020.109287,
        2020b.

Irigoien, X. and Castel, J.: Light limitation and distribution of chlorophyll pigments in a highly turbid estuary: The Gironde (SW France),
        Estuarine, Coastal and Shelf Science, 44, 507–517, https://doi.org/10.1006/ecss.1996.0132, 1997.

Kromkamp, J. and Peene, J.: Possibility of net phytoplankton primary production in the turbid Schelde Estuary (SW Netherlands), Marine
545   Ecology Progress Series, 121, 249–259, https://doi.org/10.3354/meps121249, 1995.

Le Coz, M., Chambord, S., Meire, P., Maris, T., Azémar, F., Ovaert, J., Buffan-Dubau, E., Kromkamp, J. C., Sossou, A. C., Prygiel,
        J., Spronk, G., Lamothe, S., Ouddane, B., Rabodonirina, S., Net, S., Dumoulin, D., Peene, J., Souissi, S., and Tackx, M.: Test of
        some ecological concepts on the longitudinal distribution of zooplankton along a lowland water course, Hydrobiologia, 802, 175–198,
        https://doi.org/10.1007/s10750-017-3256-6, 2017.

550 Lionard, M., Azémar, F., Boulêtreau, S., Muylaert, K., Tackx, M., and Vyverman, W.: Grazing by meso- and microzooplankton on phy-
        toplankton in the upper reaches of the Schelde estuary (Belgium/The Netherlands), Estuarine, Coastal and Shelf Science, 64, 764–774,
        https://doi.org/10.1016/J.ECSS.2005.04.011, 2005a.

Lionard, M., Muylaert, K., Van Gansbeke, D., and Vyverman, W.: Influence of changes in salinity and light intensity on growth
        of phytoplankton communities from the Schelde river and estuary (Belgium/The Netherlands), Hydrobiologia, 540, 105–115,
555   https://doi.org/10.1007/s10750-004-7123-x, 2005b.

Liu, B. and de Swart, H. E.: Impact of river discharge on phytoplankton bloom dynamics in eutrophic estuaries: A model study, Journal of
        Marine Systems, 152, 64–74, https://doi.org/10.1016/j.jmarsys.2015.07.007, 2015.

Liu, B., de Swart, H. E., and de Jonge, V. N.: Phytoplankton bloom dynamics in turbid, well-mixed estuaries: A model study, Estuarine,
        Coastal and Shelf Science, 211, 137–151, https://doi.org/10.1016/j.ecss.2018.01.010, 2018.

560 Lucas, L. V., Cloern, J. E., Koseff, J. R., Monismith, S. G., and Thompson, J. K.: Does the Sverdrup critical depth model explain bloom
        dynamics in estuaries?, Journal of Marine Research, 56, 375–415, https://doi.org/10.1357/002224098321822357, 1998.

Maes, J., Stevens, M., and Ollevier, F.: The composition and community structure of the ichthyofauna of the upper Scheldt estuary: synthesis of a 10-year data collection (1991-2001), Journal of Applied Ichthyology, 21, 86–93, https://doi.org/10.1111/j.1439-0426.2004.00628.x, 2005.

565 Maris, T. and Meire, P.: OMES rapport 2016. Onderzoek naar de gevolgen van het Sigmaplan, baggeractiviteiten en havenuitbreiding in de Zeeschelde op het milieu., Tech. Rep. Report Ecosystem Management Research Group ECOBE, 017-R206, University of Antwerp, Antwerp, Belgium, www.vliz.be/imisdocs/publications/310259.pdf, 2017.

Meire, P., Ysebaert, T., Van Damme, S., Van den Bergh, E., Maris, T., and Struyf, E.: The Scheldt estuary: a description of a changing ecosystem, Hydrobiologia, 540, 1–11, https://doi.org/10.1007/s10750-005-0896-8, 2005.

570 Mialet, B., Azémar, F., Maris, T., Sossou, C., Ruiz, P., Lionard, M., Van Damme, S., Lecerf, A., Muylaert, K., Toumi, N., Meire, P., and Tackx, M.: Spatial spring distribution of the copepod Eurytemora affinis (Copepoda, Calanoida) in a restoring estuary, the Scheldt (Belgium), Estuarine, Coastal and Shelf Science, 88, 116–124, https://doi.org/10.1016/j.ecss.2010.03.018, 2010.

Mialet, B., Gouzou, J., Azémar, F., Maris, T., Sossou, C., Toumi, N., Van Damme, S., Meire, P., and Tackx, M.: Response of zooplankton to improving water quality in the Scheldt estuary (Belgium), Estuarine, Coastal and Shelf Science, 93, 47–57,
575 https://doi.org/10.1016/j.ecss.2011.03.015, 2011.

Muylaert, K. and Sabbe, K.: Spring phytoplankton assemblages in and around the maximum turbidity zone of the estuaries of the Elbe (Germany), the Schelde (Belgium/The Netherlands) and the Gironde (France), Journal of Marine Systems, 22, 133–149, https://doi.org/10.1016/S0924-7963(99)00037-8, 1999.

Perkin, R. G. and Lewis, E. L.: The Practical Salinity Scale 1978: Fitting the Data, IEEE Journal of Oceanic Engineering, 5, 9–16,
580 https://doi.org/10.1109/JOE.1980.1145441, 1980.

Platt, T., Gallegos, C. L., and Harrison, W. G.: Photoinhibition of Photosynthesis in Natural Assemblages of Marine-Phytoplankton, Journal of Marine Research, 38, 687–701, http://biblioimarpe.imarpe.gob.pe:8080/bitstream/handle/123456789/1357/BOL%20EXTR. %20Investigaci%C3%B3n%20....-18.pdf?sequence=1, 1980.

Rice, E. W., Baird, R. B., Eaton, A. D., and editors: Standard Methods for the Examination of Water and Wastewater, American Public Health
585 Association, American Water Works Association, and Water Environment Federation, 23rd edn., 2017.

Rijkswaterstaat: Rijkswaterstaat official website, https://www.rijkswaterstaat.nl/english/index.aspx, 2020.

Soetaert, K., Herman, P., and Kromkamp, J.: Living in the Twilight - Estimating Net Phytoplankton Growth in the Westerschelde Estuary (the Netherlands) by Means of an Ecosystem Model (moses), Journal of Plankton Research, 16, 1277–1301, https://doi.org/10.1093/plankt/16.10.1277, 1994.

590 Soto, D. and Hurlbert, S. H.: Long-Term Experiments on Calanoid-Cyclopoid Interactions, Ecological Monographs, 61, 245–266, https://doi.org/10.2307/2937108, 1991.

Sverdrup, H. U.: On Conditions for the Vernal Blooming of Phytoplankton, ICES Journal of Marine Science, 18, 287–295, https://doi.org/10.1093/icesjms/18.3.287, 1953.

Tackx, M. L., Herman, P. J., Gasparini, S., Irigoien, X., Billiones, R., and Daro, M. H.: Selective feeding of Eurytemora affinis
595 (Copepoda, Calanoida) in temperate estuaries: Model and field observations, Estuarine, Coastal and Shelf Science, 56, 305–311, https://doi.org/10.1016/S0272-7714(02)00182-8, 2003.

Tilman, D., Kilham, S. S., and Kilham, P.: Phytoplankton Community Ecology: The Role of Limiting Nutrients, Annual Review of Ecology and Systematics, 13, 349–372, https://doi.org/10.1146/annurev.es.13.110182.002025, 1982.

Vegter, F. and De Visscher, P. R. M.: Phytoplankton primary production in Brackish Lake Grevelingen (SW Netherlands) during 1976-1981,
600   Netherlands Journal of Sea Research, 18, 246–259, https://doi.org/10.1016/0077-7579(84)90004-8, 1984.

Warner, J. C., Geyer, W. R., and Lerczak, J. A.: Numerical modeling of an estuary: A comprehensive skill assessment, Journal of Geophysical
      Research: Oceans, 110, 1–13, https://doi.org/10.1029/2004JC002691, 2005.

Waterinfo.be: Measurements and predictions of Waterinfo.be [DATA], [Available online at https://www.waterinfo.be/], cited 2019.

Winkler, G., Dodson, J. J., Bertrand, N., Thivierge, D., and Vincent, W. F.: Trophic coupling across the St. Lawrence river estuarine transition
605   zone, Marine Ecology Progress Series, 251, 59–73, https://doi.org/10.3354/meps251059, 2003.

Winterwerp, J. C.: On the flocculation and settling velocity of estuarine mud, Continental Shelf Research, 22, 1339–1360,
      https://doi.org/10.1016/S0278-4343(02)00010-9, 2002.